



OPEN ACCESS

EDITED BY

Emanuel Willert,
Technical University of Berlin, Germany

REVIEWED BY

Saša Milojević,
University of Kragujevac Faculty of Engineering,
Serbia
Paweł Tomczyk,
Wrocław University of Environmental and Life
Sciences, Poland

*CORRESPONDENCE

Sailesh Chitrakar,
✉ sailesh@ku.edu.np
Hari Prasad Neopane,
✉ hari@ku.edu.np

RECEIVED 11 November 2024

ACCEPTED 28 November 2024

PUBLISHED 20 December 2024

CITATION

Shrestha R, Gurung P, Chitrakar S, Thapa B,
Neopane HP, Guo Z and Qian Z (2024) Review
on experimental investigation of sediment
erosion in hydraulic turbines.
Front. Mech. Eng. 10:1526120.
doi: 10.3389/fmech.2024.1526120

COPYRIGHT

© 2024 Shrestha, Gurung, Chitrakar, Thapa,
Neopane, Guo and Qian. This is an open-access
article distributed under the terms of the
[Creative Commons Attribution License \(CC BY\)](https://creativecommons.org/licenses/by/4.0/).
The use, distribution or reproduction in other
forums is permitted, provided the original
author(s) and the copyright owner(s) are
credited and that the original publication in this
journal is cited, in accordance with accepted
academic practice. No use, distribution or
reproduction is permitted which does not
comply with these terms.

Review on experimental investigation of sediment erosion in hydraulic turbines

Rakish Shrestha^{1,2}, Prithivi Gurung^{1,2}, Sailesh Chitrakar^{1,2*},
Bhola Thapa², Hari Prasad Neopane^{2*}, Zhiwei Guo¹ and
Zhongdong Qian¹

¹State Key Laboratory of Water Resources Engineering and Management, Wuhan University, Wuhan, China, ²Department of Mechanical Engineering, Kathmandu University, Dhulikhel, Nepal

Sediment erosion in turbine materials is caused by various flow phenomena. The study of these phenomena can identify suitable measures to minimize their effect on the turbine. Various experimental test rigs have been developed alongside numerical analysis to study erosion and predict wear. In hydraulic turbines, erosion in Francis turbines is mostly seen at the guide vanes and runners, and in Pelton turbines, the needle and the bucket regions are the most vulnerable components. Prediction of wear due to erosion in various parts of the turbine is difficult, as wear depends on the properties of flow, base material, and sediment. Past studies have shown that the test rigs developed to investigate erosion have considered reducing the number of independent parameters to simplify the experiment. Erosion rates and wear patterns are predicted through both quantitative and qualitative methods. This article aims to conduct a systematic review of experimental setups and the results of those studies. This work is expected to be useful in understanding the vulnerable areas of erosion in hydraulic turbines and different mathematical relationships developed to quantify erosion, as well as to know the contemporary understanding in the sector of experimental investigation of sediment erosion.

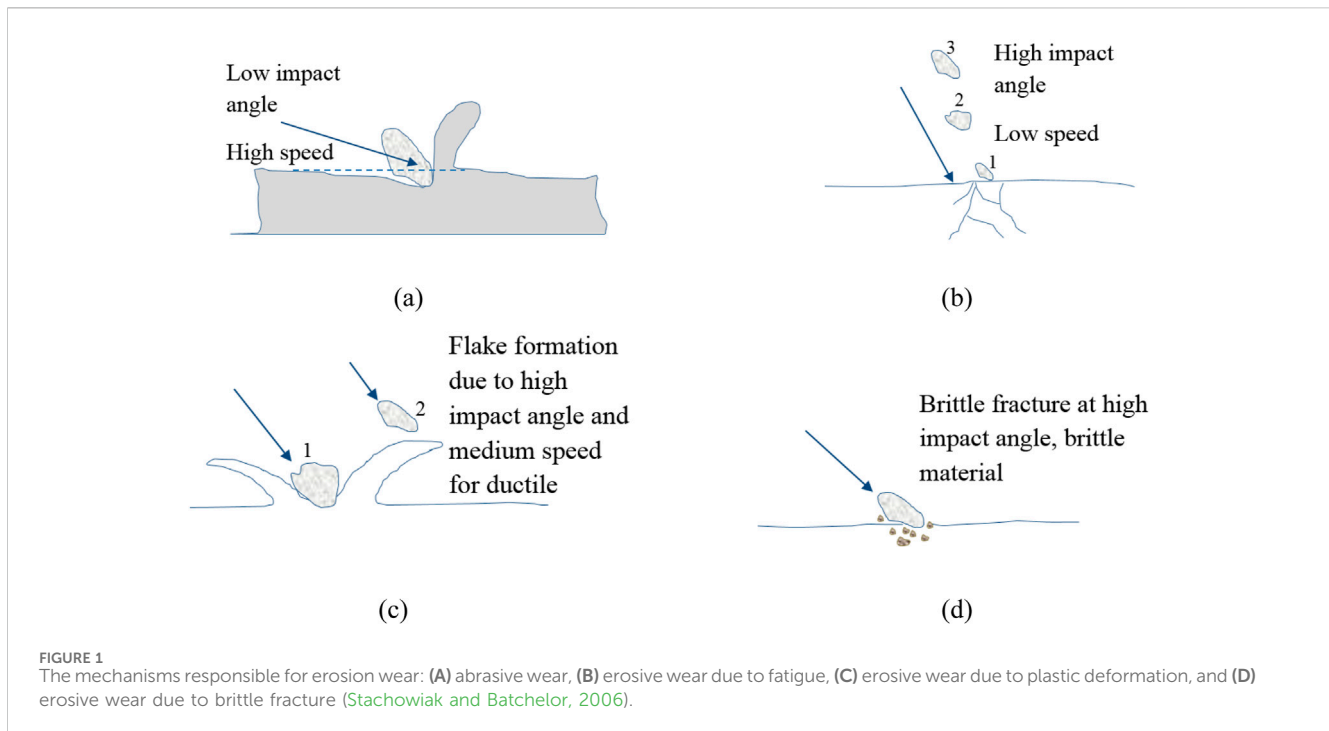
KEYWORDS

Francis turbine, Pelton turbine, sediment erosion in turbine, experimental test setups, erosion models, material wear

1 Introduction

Sediment erosion is a continuous process as the unwavering force of water disrupts the shape of rocks, causing the swift-flowing river to carry the sediments along its path. These sediments are a formidable challenge in hydropower plants as they cause abrasive and erosive wear in hydropower components and are very difficult to track, especially the

Abbreviations: ADM, acoustic discharge measurement; ANN, artificial neural network; CFD, computational fluid dynamics; CG, clearance gap; ETC-HM, erosion test system for hydraulic machinery; FFT, Fast Fourier transform; GRA, gray relational analysis; GV, guide vane; HP, hydropower; HVOF, high-velocity oxygen fuel; IEC, International Electrotechnical Commission; IGC, induction generator controller; NACA, National Advisory Committee for Aeronautics; NGV, needle guide vortex; PIV, particle image velocimetry; PLC, programming logic control; SSM, suspended sediment monitor; TOPSIS, technique for order of preference by similarity to ideal solution; UFM, ultrasonic flowmeter; VFD, variable frequency drive.



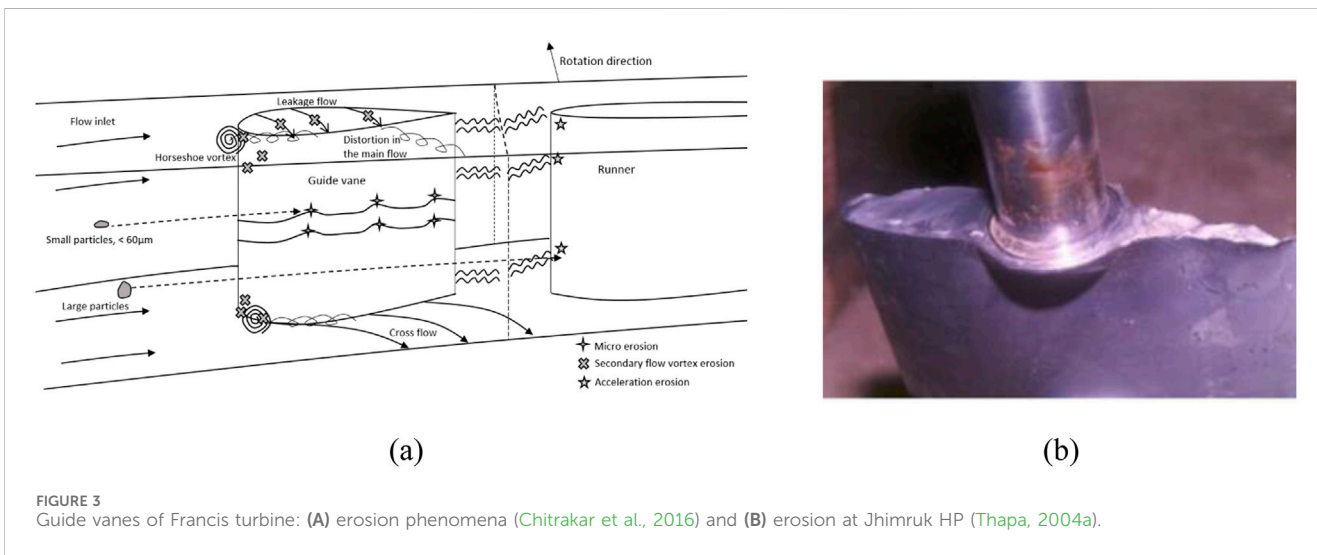
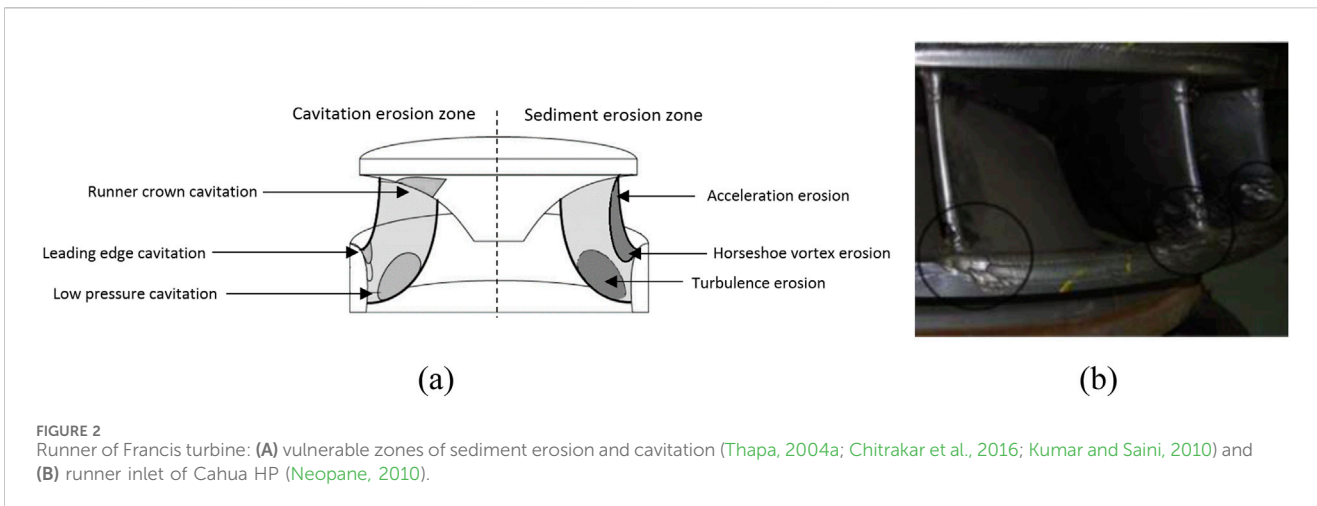
sediment particles with small size and high hardness like quartz and feldspar with Mohr's hardness at approximately 7 (Kapali et al., 2019). Along with the huge hydropower potential in the Himalayan rivers, sediments are most prominent in these rivers due to the young topography, rugged and steep terrain, and constant weathering (Neopane et al., 2019; Morin et al., 2018). Not only in the Himalayas, but sediment-loaded water flow in rivers is also a major challenge in the Andes, Alps, and the Pacific ranges with extreme flooding due to climate changes resulting in high sediment concentration during the rainy season (Winkler, 2014).

Hydro-abrasive erosion mostly affects high-head Pelton and Francis turbines because these turbines' components are exposed to extremely high velocity flows as the hydropower plant's head values increase. In certain cases, a turbine may have significant damage even after one monsoon season. Some hydropower components, such as settling basins, trash racks, desilting basins, and flushing gates, can filter sediments, but these components are usually only designed to filter out sediments larger than 200 μm (Thapa, 2004a). Sediments smaller than 200 μm cannot be removed by filtering. The turbine components get eroded when highly accelerated water flow carrying these sediments strikes the turbine. The materials used in turbines are frequently exposed to sediments that degrade their structure and functionality. As a result, sediment erosion causes efficiency loss over time, vibration, cavitation, and increased maintenance costs (Dahlhaug et al., 2010; Chhetry and Rana, 2015).

Erosion in turbine materials is one form of wear. The rate at which material is lost due to wear is influenced by various aspects such as the shape of the surfaces involved, the way they interact, the characteristics of the materials, the applied force and pressure, the environmental conditions like temperature and humidity, the surrounding atmosphere, the properties of the surfaces, and the relative speeds at which they interact (Thapa, 2004a). Turbine material wear is classified as erosive wear and abrasive wear.

Erosive wear is generated due to the impact of small particles at a high angle of attack. Depending upon the material and erodent speed, the erosive wear could be fatigue erosion if the speed is low, plastic deformation if the speed is medium for ductile material, and brittle fracture if the material is brittle. Corrosion in turbine materials also causes damage fatigue in turbine materials. In contrast, as illustrated by Figure 1, abrasive wear results from the impact of big particles at a low angle of attack (Stachowiak and Batchelor, 2006; Burwell, 1957). Supplementary Table S1 shows a brief comparison between the Francis and Pelton turbine with Supplementary Figure S1. S2.

Francis turbines are the most general hydropower turbine type around the world, with an operation range of low to medium head conditions (Kaunda et al., 2014). A Francis turbine operates with a guide vane controlling the flow going into the runner, which rotates at a certain number of revolutions per unit of time. A Francis turbine is a mixed-flow reaction turbine with the water flowing in the runner radially and exiting axially; the turbine is completely submerged in water (Bansal, 2010). As it is a reaction turbine, the turbine runner rotates due to the pressure energy and partially due to the kinetic energy. The most affected parts of this turbine due to erosion are runner blades, guide vanes, stay vanes, facing plates, and labyrinth seals (Aslam Noon and Kim, 2017). There are four different types of erosion in the guide vanes: turbulence erosion is the erosion at the guide vane (GV) outflow caused by a high fine particle velocity; secondary flow erosion is brought on by the horseshoe vortex formed by secondary flow from the clearance gap; leakage erosion occurs at the clearance gap as a result of the water's rapid acceleration; and acceleration erosion occurs as a result of the coarse particles as the water rotates in front of the runner (Chitrakar et al., 2016; Chitrakar, 2018). There are three different types of erosion in the runner: turbulence erosion, which occurs when tiny particles exit the runner at high speed; acceleration



erosion, which occurs when high acceleration occurs at the blade inlet, wrong stagnation angle erosion and leakage flow vortex filament; and cross-flow erosion, which is erosion resulting from blade tilting-induced cross flow from the hub and shroud (Chitrakar et al., 2019; Chitrakar et al., 2017a). Erosion between the rotating and stationary parts of the labyrinth seal is due to unstable leakage and turbulent flow (Brekke et al., 2002; Chitrakar et al., 2018). Figures 2, 3 show the erosion effects at the Francis turbine runner and guide vane (Chitrakar et al., 2016; Kumar and Saini, 2010; Neopane, 2010).

Pelton turbines are impulse-type turbines. Pelton turbines are used in hydropower plants in regions with high-head water resources and low flow rates, which are common in the Himalayas. The Himalayas have very high sediment concentrations with excessive composition of hard minerals, giving rise to severe sediment erosion problems. The main components affected by sediment erosion are the injector system and runner buckets. The main reasons for the accretion of sediment erosion problems in Pelton turbines are accelerated flows, turbulent flows, and vortex formations (Brekke, 2002). The injector system includes a needle, seat rings, and nozzle casing. In real cases, the

formation of a needle guide vortex (NGV) downstream of the needle guide with secondary flow phenomena, plus the acceleration in the contraction region, leads to severe hydro-abrasive erosion in the injector system (Guo et al., 2020; Bajracharya et al., 2019). The erosion severity in Pelton turbines also depends on the needle opening and is more susceptible to erosion for low openings (Chongji et al., 2014; Messa et al., 2019). The erosion in buckets is mainly due to the direct contact of waterjet and sediment particles flowing into runner buckets with high velocity. The main regions of runner buckets susceptible to erosion are the cutout regions, the splitter, and the near outlet (Bajracharya et al., 2008; Bajracharya et al., 2020; Guo et al., 2021; Ge et al., 2021). Erosion in runner buckets gets aggravated with very high particle accumulation and separation in sharp curvatures (Guo et al., 2021). The cutout back region gets the first direct impact of the water jet with very high velocity, making it most vulnerable to erosion (Guo et al., 2021). Similarly, as the flow and bucket motion progress, the splitter of the runner buckets divides the jet into two halves toward the curvatures of the bucket to change the direction of flow and extract forces from the water jet. The sediment particles also have a direct impact on the splitter of the runner buckets (Ge et al., 2021; Leguizamón

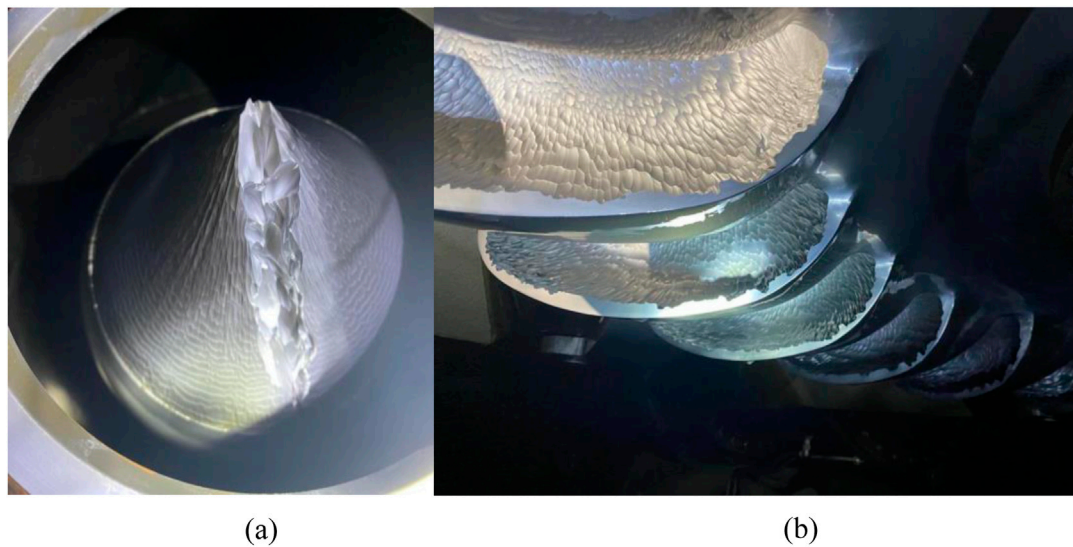


FIGURE 4
Erosion in Pelton turbine: (A) injector system and (B) bucket [Pic. S. Chitrakar].

et al., 2019). The larger sediments affect the starting sections of the runner bucket curvature due to easy and early separation from the waterjet flow. Similarly, smaller sediment affects the end sections of the curvature (near-outflow regions) of the runner buckets due to the lower capability of separation from the flow (Guo et al., 2021; Thapa, 2004b). Figure 4 shows the erosion in the injector system and bucket of a Pelton turbine.

The discussion above shows the importance of developing wear and erosion models so that erosion can be predicted. Predicting wear is challenging as the wear depends upon factors such as material properties, sediment properties, attacking angle of sediments, failure mechanisms, etc. Many diverse variables and constants have been used to predict these erosions (Meng' and Ludema, 1995). Essentially, the turbine material is exposed to a complex mechanism of friction and wear, which also represents a complex tribological phenomenon. Even though the necessary factors for hydro-abrasive erosion have been determined, the precise point at which these characteristics lead to erosion caused by hydro-abrasion is still unclear.

Corrosion due to water flow significantly impacts the durability and efficiency of hydraulic turbines, especially in harsh or sediment-laden environments. A comprehensive approach that includes optimized material selection, advanced designs, and proactive maintenance is essential to mitigate these effects and ensure long-term operational efficiency (Predescu et al., 2019). Given that the turbine blades in a water turbine are constantly exposed to water and dynamic forces, they need high corrosion resistance and strength. During the load transition, variations in the turbine and other components can create stresses and vibrations, leading to stresses and, ultimately, fatigue cracks occurring due to easy corrosion in such regions (Kumar and Singal, 2015). Corrosion is one of the possible causes of degradation of the runner blade assembly besides cavitation wear, abrasion wear, fatigue, and material defects. The main causes of corrosion and defects in hydraulic metal structures include corrosion, cavitation, and erosion wear (Niu et al., 2020). The other factors rather than defects, wear, and surface heterogeneities responsible for corrosion might be physical factors, such

as temperature, pH, and salinity of the environment, and chemical factors, such as high levels of chloride ions or dissolved oxygen (Predescu et al., 2019). The electrochemical contribution of the environment can also act together with the erosion and cavitation phenomenon to enhance the degradation mechanisms.

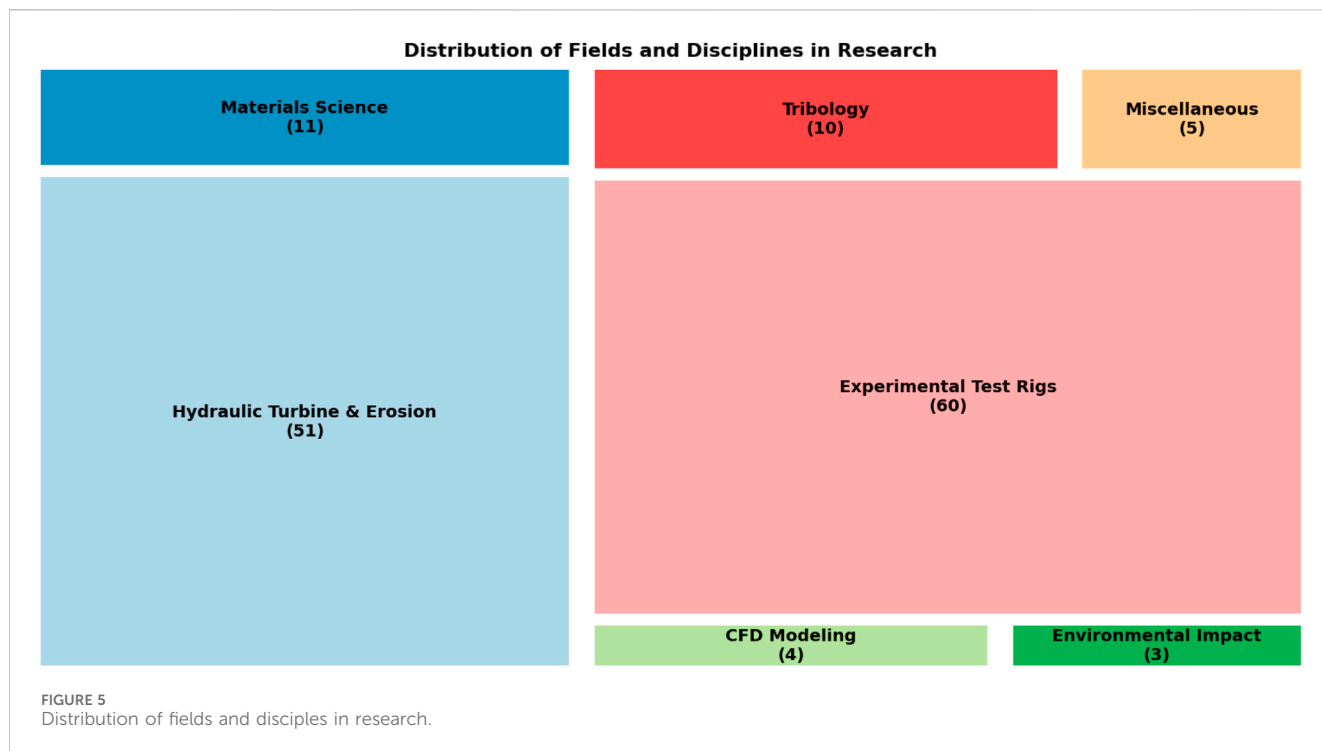
This review covers the experimental test rigs, empirical relationships, and the qualitative studies conducted on erosion, prioritizing the erosion wear effects in Francis and Pelton turbines. These studies are important because erosion occurs in the runner and guide vanes of the Francis turbine due to their complex geometry and operation under mixed-flow conditions. Pelton turbines, operating with high-velocity water jets, experience erosion on their buckets, especially in high-head applications. Understanding erosion mechanisms in both turbines helps improve efficiency, durability, and maintenance approaches in sediment-rich environments (Zhang and Zhang, 2014; Mirza Umar et al., 2024).

2 Method

For the most part, Francis and Pelton turbines have been used in experimental test rigs set up to study erosion in hydraulic turbines. The research articles related to the experiments conducted in these experimental test rigs were collected in Mendeley Reference Manager to address the following research questions:

- What experimental techniques are applied in test rigs to evaluate erosion in hydraulic turbines?
- How do experimental techniques predict the erosion wear in hydraulic turbines?
- Can experimental test rigs predict erosion similar to that observed in actual turbines?

Sediment erosion problems are more prevalent in the hydropower plants developed in rivers in the Himalayas, the



Andes, and the Alps. Most of the articles reviewed considered erosion in the hydraulic turbines of these regions. The bubble chart shown in [Supplementary Figure S3](#) illustrates the research included from different regions around the world. Most articles reviewed were from Nepal, followed by India and China. Some of the important erosion models were developed in Japan and Pakistan. The remaining articles were from South American countries like Brazil, Chile, and Colombia, where sediment erosion is prevalent, and from some European countries. Most of the articles included centered around the wear and erosion in the turbine, the materials used in the turbine, and experimental test rigs, which are also illustrated in [Figure 5](#). Some included articles provide information about the Francis and Pelton turbines and hydropower plants in general.

3 Experimental studies

Numerous numerical and experimental studies have been conducted to analyze the sediment erosion in hydro-turbines. These studies have helped develop a mathematical relationship between the sediment erosion parameters and different hydraulic components ([Thapa, 2004a](#); [Neopane, 2010](#); [Padhy and Saini, 2009](#); [Bajracharya et al., 2006](#); [Wood, 1999](#); [Thapa et al., 2021a](#)). Numerical analysis, like computational fluid dynamics (CFD), is gaining popularity with recent computational advances. However, those approaches were developed on simplified assumptions about material behavior, fluid flow patterns, or boundary conditions that introduce uncertainties. Experimental investigation gives a real-world representation to provide a more accurate understanding of the erosion process and material degradation understanding, but it could be expensive and difficult to implement. Erosion and wear

TABLE 1 Classification of erosion test rigs in terms of their working principle ([Thapa, 2004a](#); [Neopane, 2010](#); [Goyal et al., 2012](#); [Thapa et al., 2012b](#)).

Jet type test rig	Rotating disc/arm type rig
Jet erosion test rig	Rotating disc apparatus (RDA)
Guide vane cascade rig	Pot erosion tester
Pelton turbine test rig	Francis turbine test rig

have a major effect on turbine lifetime and performance. Other high-load, high-friction systems, such as internal combustion engine compressors, have been found to have comparable difficulties. [Milojević et al. \(2023\)](#) looked at aluminum alloys reinforced with cast iron and anti-friction coatings to lower friction and wear in reciprocating air compressors, leading to noticeable durability. Potential remedies, in addition to ceramic coatings for reducing wear in turbine components, may be provided by such material changes and surface treatments. The study of sediment erosion in turbine materials in lab conditions could be categorized into two main categories ([Thapa, 2004a](#); [Wood and Wheeler, 1998](#)) based on the working principles which are: (a) a jet erosion type test rig and (b) a rotating disc type test rig. [Table 1](#) shows the division of test rigs in terms of their working principles.

3.1 Jet erosion test rigs

A jet erosion test rig is an experimental rig to evaluate the erosion resistance of materials when subjected to sediment and water or air ([Karthik and Amarendra, 2019](#)). The major components are the jet nozzle, from where the high-speed water jet is directed to

the test sample; a test chamber, where the sample is placed and is subjected to the water jet; and the water supplier, which includes the pumps and pipes to deliver water at a controlled pressure and flow rate. The model also includes a sample holder to hold the sample materials correctly, measuring instruments such as the high-speed camera to observe the erosion process, and a control system to control the test parameters such as the velocity of the jet. Neilson and Gilchrist (1967) studied sediment erosion on a material of aluminum, glass, Perspex, and carbon plates from sediment-laden gas streams. They examined the impacts of particle shape, velocity, and angle of attack through experimental results on various specimen materials with varying physical characteristics. A simple theoretical analysis is provided to correlate the experimental data, allowing the prediction of erosion characteristics at different angles of attack for various materials. This was one of the early experimental setups of a jet erosion test rig for erosion testing. Elkholy (1983) studied the abrasive wear on the materials of slurry pumps, which are aluminum and cast iron, with Brinell hardness values of 121 and 230, respectively. A jet abrasion test facility was developed for the experiment with components such as a test tank, specimen holder, sand entrance, nozzle, centrifugal pump, pressure gauge, air supply, variable speed motor, weight scale, and sample nozzle. The varying parameters for the experiment were the velocity of the jet, the impingement angle, sediment with different hardness, such as silica sand, sediment particle size, and sediment concentrations. The wear resistance erosion model of cast iron was predicted from the experiment. Wiederhorn and Hockey (1983) conducted erosion analysis on several materials to observe how they eroded, compared the materials in terms of erosion rate at various particle velocities, and developed a general wear rate equation.

Turenne et al. (1989) utilized a jet erosion test rig configuration to study erosion on test materials and discovered that slurry erosion is dependent on the fluid's characteristics, the erodent's properties, operation settings, and the properties of the materials to be evaluated. A fixed number of sediments was introduced to a water tank, and the mixture was circulated using an air-powered slurry pump. Thapa et al. (2005) developed a slurry jet erosion test rig in which a container with sediment is located along the main flow line where water is propelled by a centrifugal pump that disturbs the sediments at the container controlled by the valve. The material to be tested is kept at the container. Haugen et al. (1995) studied the erosion damage brought on by sand particles in oil and gas production equipment, notably choke valves. That study emphasizes the significance of maximizing design and using erosion-resistant materials to increase the longevity of these components. The study tested 28 different materials for erosion resistance, including tungsten carbide, coatings, ceramics, and several grades of steel. The findings show that choosing the proper material may boost a component's lifespan by a factor of over 10. Choke valve design optimization can also result in considerable financial savings.

Erosion modeling with computational fluid dynamics is essential to anticipate erosion rates and sites. The research highlighted the importance of material selection and design optimization in lessening erosion damage in offshore oil and gas production equipment. Karthik and Amarendra (2019) developed a slurry erosion test rig based on the concept of a Venturi meter.

Sediments are injected into the main flow from the funnel. The test specimen, brass, was subjected to erosion at different impingement angles from 0° to 90°, once with clear water erosion and once with slurry erosion. Because it is a ductile material, brass was found to erode more at the 30° impingement angle in both conditions. The water erosion test was conducted for 10 min, and the slurry erosion test was conducted for 1 min. Scanning electron microscope (SEM) results revealed that the slurry erosion created more microcracks in only a minute at all impingement angles. Yan et al. (2020) developed a model to estimate the rate of erosion of titanium alloy blades in a sediment-laden environment while taking into account the effects of sand fracture, particle size, and velocity. The erosion models obtained from the experiments based on a jet tester are listed in Table 2. The details about the test conditions and turbine material are shown in Supplementary Table S2. Figures 6A, B show the experimental setup of high-speed sand erosion; the components of the test rig are a gas inlet from where the air is injected, a sand feeding device to inject sand into the test chamber where the test material for the erosion to be tested is fixed (Yan et al., 2020; Burstein and Sasaki, 2000). Supplementary Tables S4A, B show the jet test rig injector system employed by Zu et al. (1990), Lin et al. (2006), and Santa et al. (2009).

3.2 Pot erosion testers

Another type of erosion test rig used to examine how different materials behave when subjected to varying solid concentrations, impacts, and impact angles is the pot tester (More et al., 2014). As shown in Figure 13, the experimental setup comprises a revolving main shaft with test samples and a slurry pot unit with a pot. The motor is attached at the end of the shaft, which is installed on the lid. Using a specially designed testing setup, Tsai et al. (1981) determined that it was possible to see the faster degradation of three different steel alloys caused by coal and SiC in kerosene. An experiment was conducted to measure erosion rates, and dimensional analysis was used to correlate the results. Empirical constants were determined through regression analysis. The experiments revealed the effects of factors like particle velocity, density, concentration, hardness, temperature, and fluid mechanics on the erosion of materials. De Bree et al. (1982) created one of the first configurations for the pot erosion tester, which consisted of two horizontal discs with four specimens within, spinning in opposing directions on concentric vertical shafts. One such pot tester designed by W.J. Schumacher had three hubs, which could individually support eight specimens on a vertical plane while the specimens were being transported through silt-eroded particles in a stationary slurry (Schumacher, 1987). This type of erosion tester was used to characterize erosion and select appropriate materials.

The impact of solid particles suspended in a fluid on a material surface results in slurry erosion. Slurry erosion test rigs simulate this process by pumping a slurry mixture onto the test material, typically using a slurry jet or a rotating impeller. Control over aspects such as impact velocity, solid particle concentration, and impact angle is possible with the jet impingement slurry erosion test setup. There are two main types of slurry erosion test methods: laboratory simulation testing and pipe wear tests. Although pipeline testing offers settings more akin to those seen in actual practice, simulation

TABLE 2 Summary of erosion models based on experiments in the jet tester rig.

Name	Base materials	Erodent and solvent	Specifications of specimen	Erosion model	Description of the model
Neilson and Gilchrist (1967)	Aluminum Glass Polymer	E: Al ₂ O ₃ S: Air	N/A	$W = \frac{\frac{1}{2}M(V^2 \cos^2 \alpha - v_p^2)}{\varnothing} + \frac{\frac{1}{2}M(V \sin \alpha - K)^2}{\varepsilon}$ $\alpha < \alpha_0$ $W = \frac{\frac{1}{2}MV^2 \cos^2 \alpha}{\varnothing} + \frac{\frac{1}{2}M(V \sin \alpha - K)^2}{\varepsilon}$ $\alpha > \alpha_0$	W is the erosion produced by M kg at the angle of attack α and particle velocity V, kg s ⁻¹ K is the velocity component normal to the surface v_p is the particle velocity, m/s
Elkholy (1983)	Cast Iron	E: SiO ₂ S: Water	N/A	$\Delta W_{CI} = 1.342 \times 10^{-5} C_V^{0.682} \left(\frac{H_1}{H_2}\right)^n d^{0.616} V^{2.39} \left\{1 + \sin\left(\frac{\alpha - \alpha_1}{90 - \alpha_1}\right) 180 - 90\right\} T$	ΔW_{CI} represents the wear equation of cast iron, kg of iron/kg of sand H_1 is solid particle hardness, HB H_2 is specimen material hardness, HB n is a function of H_1/H_2 C_V is concentration by volume, kg m ⁻³ C_W is concentration by weight, kg kg ⁻¹ V is the flow velocity, m s ⁻¹ d is particle diameter, m T is the time over which wear was measured; s H_1 is the solid particle hardness, HB. H_2 is the pipe material hardness, HB. α is the impingement angle α_1 is the angle at which wear is developed
Wiederhorn and Hockey (1983)	Sintered Al ₂ O ₃ Sapphire Silicon Sintered MgO Fused silica Soda-lime-Silica glass	E: SiC grains S: Air	N/A	$W (H/K_C)^6 = A' (v^2 \rho / H)^c (RH^2 / K_C^2)^b$	W is the erosion rate, m ³ K_C is the target toughness of material, kg.s ⁻² m ^{1/2} H is the target hardness of the material, Pa $(H/K_C)^2$ is an index of brittleness v^2 is the particle energy density, that is, the kinetic energy per unit volume of the particle R is the radius of the particle impacting, m
Turenne et al. (1989)	Aluminum Glass	E: SiO ₂ S: Water	N/A	$\frac{W}{M} = \frac{4.55 \times 10^{-7}}{f^{0.33}}$	W/M is the erosion rate, kg/kg f is the sand volume fraction M is the mass of the abrasive particles impinged on the surface, kg F is the particle flux, kg m ⁻² s ⁻¹ $M = F \left(\frac{\pi d^2}{4}\right) t$
Haugen et al. (1995)	Al ₂ O ₃ PSZ (Zirconia) ZrO ₂ -Y ₃ (Ytria zirconia) Si ₃ N ₄ SiC TiB ₂ B ₄ C SiSiC	E: SiO ₂ and Al ₂ O ₃ S: Oil and gas	N/A	$E = M_p K F(\alpha) V_p^n$	E is the weight loss of the target material, mg per kg M_p is the mass of sand striking the target material, mg V_p is the particle impact velocity, m/s α is the particle impact angle, degree K and n are the constants depending on the physical characteristics of the materials. The functional relationship $F(\alpha)$ describes how erosion depends on the particle impact angle: $F(\alpha) = \sum_{i=1}^8 (-1)^{(i+1)} A_i \left(\frac{\alpha \pi}{180}\right)^i$ Where $A_1 = 9.370$, $A_2 = 42.295$, $A_3 = 110.864$, $A_4 = 175.804$, $A_5 = 170.137$, $A_6 = 98.298$, $A_7 = 31.211$, and $A_8 = 4.170$

(Continued on following page)

TABLE 2 (Continued) Summary of erosion models based on experiments in the jet tester rig.

Name	Base materials	Erodent and solvent	Specifications of specimen	Erosion model	Description of the model
Yan et al. (2020)	Ti-6Al-4V	E: Quartz S: Air	L: 0.055 m×0.025 m×0.003 m	$ER_{\alpha} = g(\alpha) \sum_{i=1}^N \frac{F_i(ER_{\alpha})}{N}$ $F(ER_{\alpha}) = K_m K_{rock} \rho_p (Hv)^{k_1} \left[\frac{F(v)D}{v} \right]^{k_2}$ $\left[\frac{F(v)D}{v} \right]^{k_3} (CF)^{k_4} g(\alpha) = (\sin \alpha)^{n_1} [1 + Hv(1 - \sin \alpha)]^{n_2}$	The angle function that influences the erosion rate is $g(\alpha)$, K is the constant with particle property, and ER_{α} is the erosion rate (mg/kg) at the angle of attack α ($^{\circ}$). The exponent factors k_1 , k_2 , and k_3 are influenced by the target hardness, velocity, and particle size. ρ_p is the material density (kg/m ³), Hv is the material hardness (GPa), and v and v' are the impact velocity (m/s) and the minimal impact velocity (m/s). The material extrusion and cutting damage exponent factors are n_1 and n_2 .

testing is still commonly used because of its low cost, ease of setup and operation, and speed of result generation (Zu et al., 1990). Gupta et al. (1995) discussed wear in a slurry pipeline with a particular emphasis on erosion wear brought on by variables such as velocity, concentration, and particle size. Wear on brass and mild steel pipes using a pot tester was noted, and connections to forecast erosion wear were made. For multi-sized slurries, the weighted mean diameter and created formulae to forecast uneven wear were calculated. Utilizing local concentration, particle size, and velocity, the concept helps in pipeline design and optimization by calculating wear in a pipeline. Pot tester data are a tool for determining the best conditions for operation and extending pipeline longevity. However, there is a lack of control over the erosion parameters. Gandhi et al. (1999) examined the erosion wear brought on by solid particle cutting in flows containing solids and liquids. The study focused on parallel flow erosion using a specifically created slurry pot tester. The studies investigated various solid concentrations, particle sizes, and velocities and showed that increasing solid concentration, particle size, and velocity results in increased parallel flow wear. Velocity has a greater impact than solid concentration or particle size. In order to anticipate the wear rate, the research tried to comprehend the details of erosion by creating correlations and improving power law connections.

Patil et al. (2011) conducted a study focusing on the wear caused by erosion of ductile materials in solid-liquid combinations, particularly on aluminum in a sand-water slurry. In the study, erosion wear was examined in relation to factors such as impact angle, particle size, velocity, and solid concentration using a pot tester. Up to a 45° impact angle, the erosion wear grew with the impact but reduced beyond that. At high impact angles, particle size displayed a linear relationship with erosion wear. The severity of the wear was positively influenced by solid concentration, although the effect weakened as concentration increased and velocity had a substantial impact on eroding wear (Naidu, 1997a). Based on the investigated factors, a correlation with a 16% error margin was created to predict erosion wear. More et al. (2014) developed a pot tester to mimic the erosion wear caused by mixtures of solid and liquid. The setup consisted of a revolving propeller and a shaft from the top with a test specimen attached that was connected to a motor to spin at different speeds from the bottom. The study concerned how AISI SS304L ductile material behaved with respect to erosion under various environmental factors. The impact angle, concentration, velocity, and impacts of particle size on wear may all be measured with the pot tester's design. In order to comprehend erosion mechanisms, eroded surfaces were subjected to SEM investigation. The results exhibit strong agreement with experimental data, allowing for a more accurate wear assessment of industrial components.

Tarodiya and Gandhi (2019) studied how the erosion rates of various materials, namely, steel 304L, gray cast iron, and high chromium white cast iron, vary in slurry conveyance systems reacting to slurry erosion using a pot tester. The effects of impact angle, particle size, and velocity on erosion were investigated. According to power law correlations, erosion rates were observed to rise with particle size and velocity. However, the erosional process

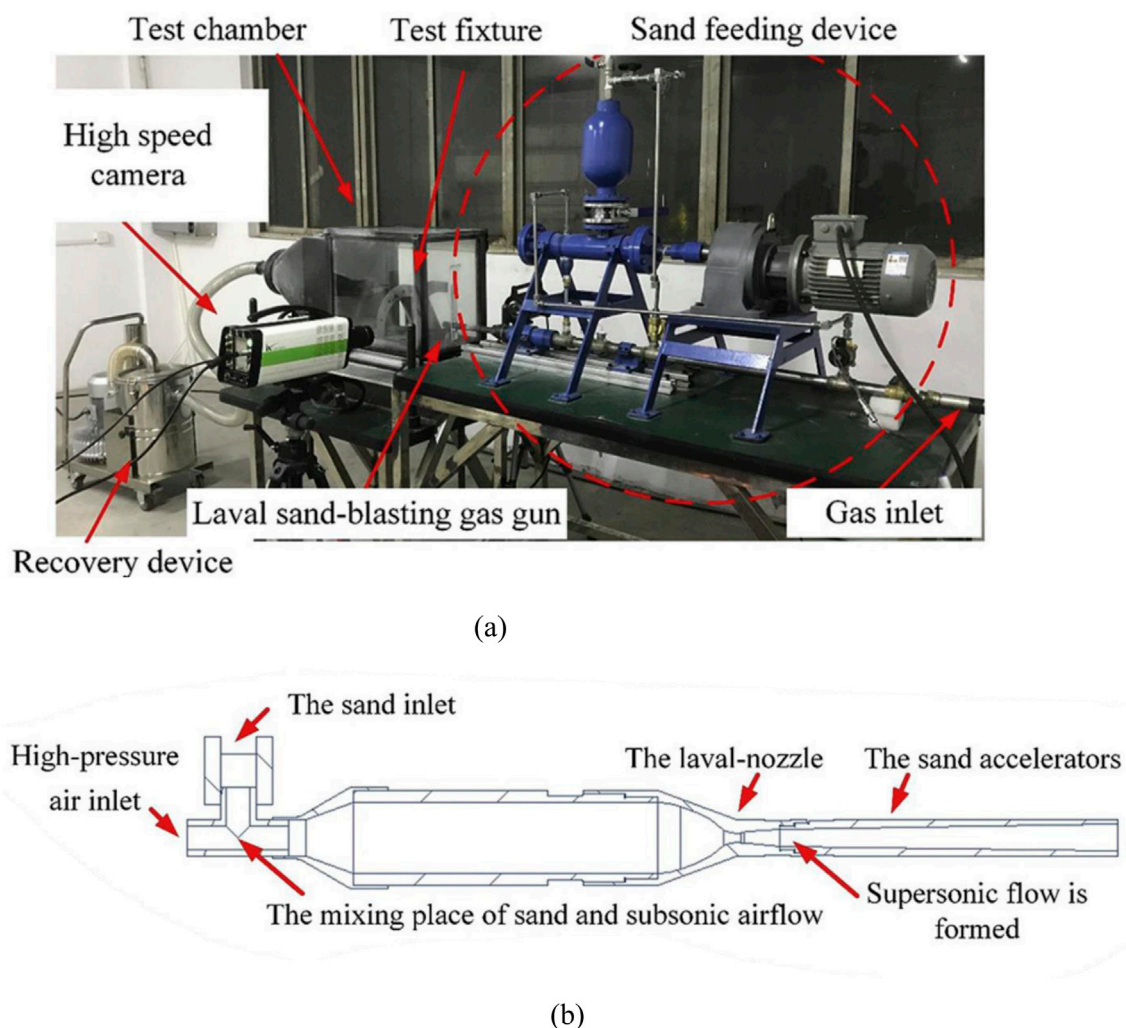


FIGURE 6 (A) Test equipment for high-speed sand erosion (Yan et al., 2020; Burstein and Sasaki, 2000). (B) Schematic diagram of the blasting nozzle (Yan et al., 2020).

remained constant with varying velocity. Correlations were made to estimate erosion rates with a maximum inaccuracy of 15%. Among the materials, white cast iron with a high chromium content demonstrated higher erosion resistance. Some of the erosion models from the study are shown in Table 3. Figure 7A, B shows the experimental setup of the pot tester, which consists of components such as rotating arms to hold the sample and rotate inside a pot that contains slurries.

3.3 Rotating disc apparatus

The rotating disc apparatus (RDA) primarily consists of a rotating disc and an electrical motor to rotate the disk (Rashed et al., 2016). A revolving disc or arm is immersed in a solution of water and sediment. Thapa et al. (2007) used an RDA to investigate the combined effects of cavitation and erosion in turbine materials. The use of an RDA for erosion and cavitation analyses is discussed separately in the following sections.

3.3.1 Rotating disc apparatus: erosion setup

Rajkarnikar et al. (2013) designed a setup to carry out erosion tests on Francis turbine runner blades of aluminum as base material using the hydraulic parameters of the Jhimruk Hydropower Plant of Nepal. The motor speed used for the experiment was 1,440 rpm, which gave a velocity of 15 m/s at the blade's inlet. The casing of the RDA was filled with sand and water. Two painted blades were mounted on the disc, and the setup was operated for about 30 min. According to Brekke (2002), the rotational motion of the fine sand particles may have caused micro erosion, which could be the cause of the erosion in the outlet region. Similar to this, obstructions in the flow course cause secondary flow vortex erosion, which is the cause of the erosion at the inlet edge (Brekke, 2002). After running the experiment for 350 min, the weight loss in the specimen and the rate of erosion were calculated, concluding that the effects of sediment erosion with different materials and coating could be compared with the RDA setup. Shrestha et al. (2021) studied the amount of erosion and erosion rate in the cross-flow turbine blade materials of SUS304, SUS440C, SUS630, SCM440, and STD11, using an RDA.

TABLE 3 Summary of erosion models based on experiments in pot tester rig.

Name	Base materials	Erodent and solvent	Specifications of specimen	Erosion model	Description of the model
Tsai et al. (1981)	A-53 MS 304 SS 316 SS	E: Coal SiC S: Kerosene	Tubular metal L: 0.05 m OD: 0.0318 m Cylindrical tank: OD: 0.20 m PD: 0.108 m M: brass	$\frac{1}{VC_p} \frac{dC_s}{dt} = A \left(\frac{\rho_p}{\rho_f}\right)^a \left(\frac{C_p}{\rho_f}\right)^b \left(\frac{S_s}{\rho_f V^2}\right)^c (13.8 \frac{S_p}{S_s})^d$ Coefficients $A = 6.32 \times 10^{-10}$ $a = 4.62$ $b = -0.54$ $c = -0.42$ $d = 0.46$ Parameter ranges $1.79 \times 10^{-10} < \frac{dC_s}{VC_p} < 9.33 \times 10^{-8}$ $1.84 < \frac{\rho_p}{\rho_f} < 3.95$ $9.80 \times 10^{-2} < \frac{C_p}{\rho_f} < 54.4 \times 10^{-2}$ $0.19 < 13.8 \frac{S_p}{S_s} < 0.99$ $8.38 \times 10^2 < \frac{S_s}{\rho_f V^2} < 5.94 \times 10^3$ $\frac{\delta}{D_p} - 1 \frac{D_p \rho_f V_p^*}{\mu_f} \approx 0$ $\frac{V_p^*}{V_p} \approx 0$	C_p is the particle concentration per unit fluid volume, kg m^{-3} $\frac{dC_s}{dt}$ is the amount of erosive wear per unit of surface erosion, $\text{kg s}^{-1} \text{m}^{-2}$ δ is the characteristic thickness of the fluid layer, m D_p is the eroding particle diameter, m S_s is the yield stress of eroded material for metals, N m^{-2} S_p is eroding particle yield stress for minerals, N m^{-2} V_p^* is the mean particle velocity function of fluid velocity, m s^{-1} V_p is the mean particle velocity's surface normal component in relation to the eroded surface, m s^{-1} ρ_f is the mass density of the fluid phase, kg m^{-3} ρ_p is the mass density of the particle phase, kg m^{-3} μ_f is the fluid viscosity, N s m^{-2}
Gupta et al. (1995)	Brass MS	E: Copper S: Water	Specimen L: 0.045 m D: 0.003 m Cylindrical tank: OD: 205 m H: 0.135 m M: aluminum	$E_{w \text{ brass}} = 0.178 V^{2.4882} d^{0.291} C_w^{0.516}$ $E_{w \text{ MS}} = 0.223 V^{2.148} d^{0.344} C_w^{0.556}$	E_w is the erosion wear, m year^{-1} W is the weight of wear, kg C_v is concentration by volume, kg m^{-3} C_w is concentration by weight, kg kg^{-1} V is the flow velocity, m s^{-1} d is the particle diameter, m T is the duration of the wear measurement, sec H_1 is the solid particle hardness, HB. H_2 is the pipe material hardness, H α is the impingement angle ^o α_1 is the angle at which wear is evolving
Clark and Wong (1995)	Pyrex glass 99.8% alumina 1020 HR steel API P110 casing steel OFHC copper Polymethylmethacrylate Acetal Phenolic	E: SiC, Alumina S: Diesel oil	Specimen D: 0.005 m	$E_T = E_C + E_D$ $E_T = \frac{1/2 M_p (V_N^2)}{\epsilon} + \frac{1/2 M_p (V_T^2 \sin 2\alpha)}{\phi}$	E_T is the total erosion E_C is the cutting erosion E_D is the deformation M_p is the total mass of colliding particles of homogeneous size At impact angle α , the particle's tangential and normal velocity components have values of V_T and V_N , respectively. Empirical constants ϵ and ϕ are associated with the unit of kinetic energy for cutting erosion and the specific energy for deformation erosion
Gandhi et al. (1999)	Brass	E: Zinc S: Water	Specimen L: 0.028 m B: 0.0065 m H: 0.002 m Cylindrical tank: OD: 0.205 m H: 0.035 m M: aluminum	$E_W = 2.57 V^{2.56} C_W^{0.83} d^{0.85}$	E_w is the erosion wear, m year^{-1} V is the flow velocity, m s^{-1} C_w is the concentration by weight ratio, kg kg^{-1} d is the particle diameter, m

(Continued on following page)

TABLE 3 (Continued) Summary of erosion models based on experiments in pot tester rig.

Name	Base materials	Erodent and solvent	Specifications of specimen	Erosion model	Description of the model																								
Patil et al. (2011)	Aluminum	E: Silica S: Water	Specimen L: 0.040 m B: 0.004 m H: 0.002 m Cylindrical tank OD: 0.245 m H: 0.15 m M: aluminum	$E_W = 0.075\theta^{0.12}C_W^{1.09}V^{3.55}d^{1.37}$	θ is the impact angle in degree C_W is the concentration by weight, % V is the velocity in m/s D is the particle size in m																								
More et al. (2014)	AISI SS304L	E: Quartz S: Water	Specimen L: 0.030 m B: 0.005 m H: 0.002 m Cylindrical tank OD: 0.24 m H: 0.225 m M: Aluminum	$E_W = E_{D(\alpha)} + E_C$ $E_{D(\alpha)} = E_{D90} (\sin \alpha)^3$ For normal impact wear $E_{D90} = 6.62 \times 10^{-14} \times K_{(H_p/H_T)} \times V^{2.02} d^{1.62} C_W^{-0.128}$ $E_C = 6.204 \times 10^{-12} \times f(\alpha) \times (MSF)^{-0.7974} (H_T)^{-0.7155} V^{2.35} d^{1.55} C_V$ $f(\alpha) = 0.9889 \left[\sin\left(\frac{\alpha}{2}\right) \left(\frac{\alpha}{\alpha_{max}}\right) \right]^{0.5898}$ for $0^\circ \leq \alpha \leq \alpha_{max}$ $f(\alpha) = 0.9186 \left[\sin\left(\frac{\pi}{2} - \left(\frac{\pi}{2}\right) \left(\frac{\alpha - \alpha_{max}}{90 - \alpha_{max}}\right)\right) \right]^{4.3044}$ for $\alpha_{max} \leq \alpha \leq 90^\circ$	V is the velocity of the impact particle, m/s d is the particle size, μm C_W is the solid particles' concentration, % by weight K is a constant that depends on the hardness ratio $K = 0.42$ for $H_p/H_T \leq 6$ (Region-I) $K = 1.0$ for $12.3 \leq H_p/H_T \leq 12.3$ (Region-II) $K = 1.83$ for $12.3 \leq H_p/H_T \leq 27.5$ (Region-III)																								
Tarodiya and Gandhi (2019)	Steel 304L Gray cast iron High chromium white cast iron	E: SiO ₂ and Fe ₂ O ₃ S: Water	Cylindrical tank D: 0.8 m H: 0.533 m M: SS	$ER = K f(\alpha) V^\beta d^\gamma$ $f(\alpha) = a_1 \left[\sin\left(\frac{\alpha}{2}\right) \left(\frac{\alpha}{\alpha_{max}}\right) \right]^{b_1}$ for $0^\circ \leq \alpha \leq \alpha_{max}$ $f(\alpha) = a_2 \left\{ \sin\left[\left(\frac{\pi}{2}\right) - \left(\frac{\pi}{2}\right) \left(\frac{\alpha - \alpha_{max}}{90 - \alpha_{max}}\right)\right] \right\}^{b_2}$ for $\alpha_{max} \leq \alpha \leq 90^\circ$ Steel 304L, $a_1 = 0.99$ $b_1 = 0.92$ $a_2 = 0.68$ $b_2 = 1.89$ Gray cast iron, $a_1 = 0.99$ $b_1 = 0.57$ $a_2 = 0.64$ $b_2 = 1.96$ High chromium white cast iron, $a_1 = 0.99$ $b_1 = 0.86$ $a_2 = 0.73$ $b_2 = 1.93$	V is the velocity of the affecting particle, m/s d is the size of the particle, μm <table border="1"> <thead> <tr> <th>Material</th> <th>Constant</th> <th>ER_c</th> </tr> </thead> <tbody> <tr> <td rowspan="3">Steel 304L</td> <td>K</td> <td>1.51×10^{-11}</td> </tr> <tr> <td>β</td> <td>2.15</td> </tr> <tr> <td>γ</td> <td>0.71</td> </tr> <tr> <td rowspan="3">Gray cast iron</td> <td>K</td> <td>4.75×10^{-14}</td> </tr> <tr> <td>β</td> <td>3.08</td> </tr> <tr> <td>γ</td> <td>1.31</td> </tr> <tr> <td rowspan="3">High chromium white cast iron</td> <td>K</td> <td>3.96×10^{-13}</td> </tr> <tr> <td>β</td> <td>2.78</td> </tr> <tr> <td>γ</td> <td>0.79</td> </tr> </tbody> </table>	Material	Constant	ER _c	Steel 304L	K	1.51×10^{-11}	β	2.15	γ	0.71	Gray cast iron	K	4.75×10^{-14}	β	3.08	γ	1.31	High chromium white cast iron	K	3.96×10^{-13}	β	2.78	γ	0.79
Material	Constant	ER _c																											
Steel 304L	K	1.51×10^{-11}																											
	β	2.15																											
	γ	0.71																											
Gray cast iron	K	4.75×10^{-14}																											
	β	3.08																											
	γ	1.31																											
High chromium white cast iron	K	3.96×10^{-13}																											
	β	2.78																											
	γ	0.79																											

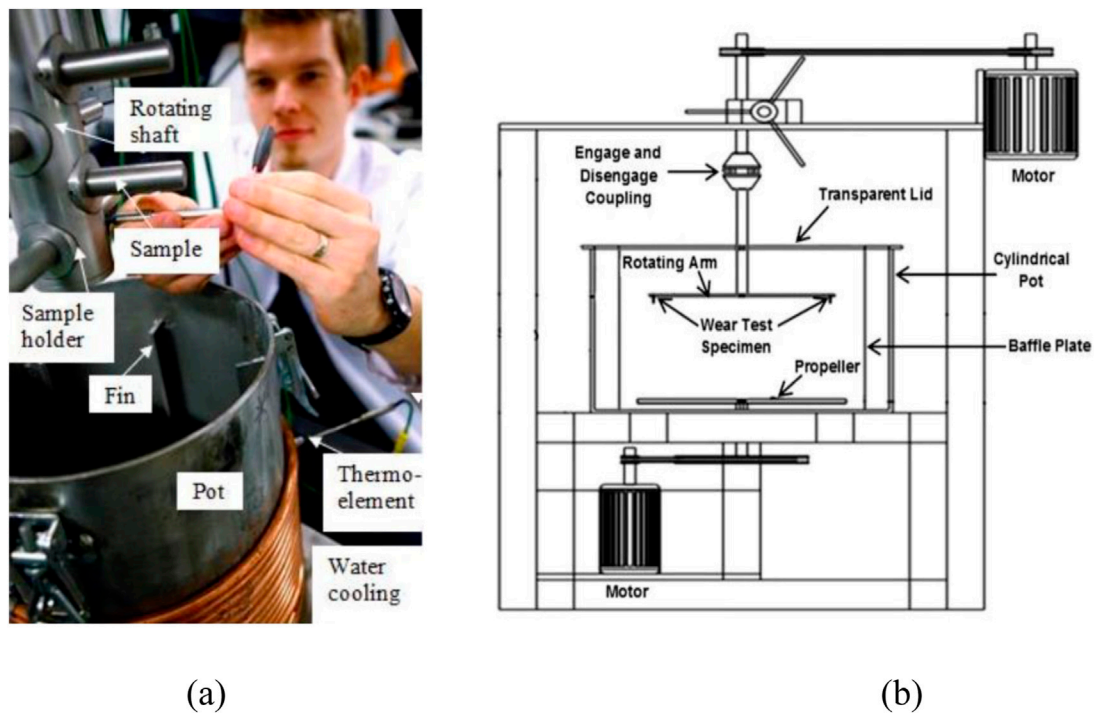


FIGURE 7 (A) Pin mill slurry-pot tester (Ojala et al., 2015). (B) Schematic diagram of slurry-pot tester (Sharma and Gandhi, 2020).

SUS304 had the highest cumulative erosion, while STD11 had the lowest. Tungsten carbide coatings improved erosion resistance for SUS304 and SUS440C but increased erosion in coated WC-STD11. Erosion rates were highest in SUS304 and lowest in STD11, generally increasing linearly with time. Flow pattern analysis showed similar velocity patterns in CFT and RDA, with differences in flow separation and vortex formation due to blade number and rotation mechanisms. A study by Aryal et al. (2022) compared the erosion patterns in a guide vane using CFD and the patterns of erosion using the RDA. The experiment in the RDA was done using a mild steel specimen in a controlled environment. The study showed that the flow region around the guide vanes in the RDA closely matches that of actual turbines and with similar stagnation points and pressure distributions. The erosion patterns observed in the RDA aligned with the CFD simulation results, particularly in high-velocity regions and areas prone to vortex formations. Acharya et al. (2022) conducted an experiment in an RDA to validate the erosion induced by the sediments in the sidewall gaps of the Francis turbine predicted by the CFD method. The experimental setup aimed to imitate the conditions defined in the numerical model. The disc rotated at 750 RPM, which is the same as the reference turbine's speed. The sediment used in the experiments had a concentration of around 50,000 parts per million (ppm), with particles having an average shape factor of 0.68 and a diameter of less than 150 μm . Two areas of erosion were seen in the experiment: the first was at the farthest end from the center of rotation, where the greatest erosion was caused by flow recirculation and centrifugal forces. The second region is less than a 90-degree angle to the slot length, where erosion was influenced by both radial and circumferential velocity components acting on the sediment

particles. Figure 8A shows the RDA experimental rig, which consists of a disc where the test sample is mounted that rotates from the torque generated by the motor. Openings include the water-in, where water enters the apparatus, and the water-out, where the water exits the setup. The sand-in opening is for adding the sand to the apparatus. Figures 8B, C show the erosion pattern observed from the experiment in the RDA and from the CFD done in ANSYS CFX v18.1 using an ICEM mesh.

3.3.2 Rotating disc apparatus: cavitation setup

Shima et al. (1992) examined stainless steel's resilience to cavitation damage in an RDA throughout a large peripheral speed range of 65–77 m/s. Using a through-hole as the cavitation inducer, the cavitation number in the research was utilized to estimate the location and extent of damage on the specimen. The erosion was observed in the regions where cavitation clouds collapsed, and higher peripheral velocities resulted in a decrease in the cavitation number at which maximum erosion occurred. According to the study, higher peripheral speeds also tend to result in an increase in the velocity exponent, which shows how much velocity affects erosion. A fixed static pressure resulted in a greater velocity exponent when compared to findings obtained with a fixed cavitation number. Under different test settings, a power law relationship between the cumulative weight loss and the weight loss rate was discovered during the erosion acceleration period, offering insights into the erosion process itself (Zhang et al., 1996). Bazanini et al. (2008) conducted an experiment to observe the cavitation pattern and quantify the mass loss due to the cavitation in an RDA. The setup consisted of a rotating metallic disk with cavity inducers, such as holes, to evaluate the effects of

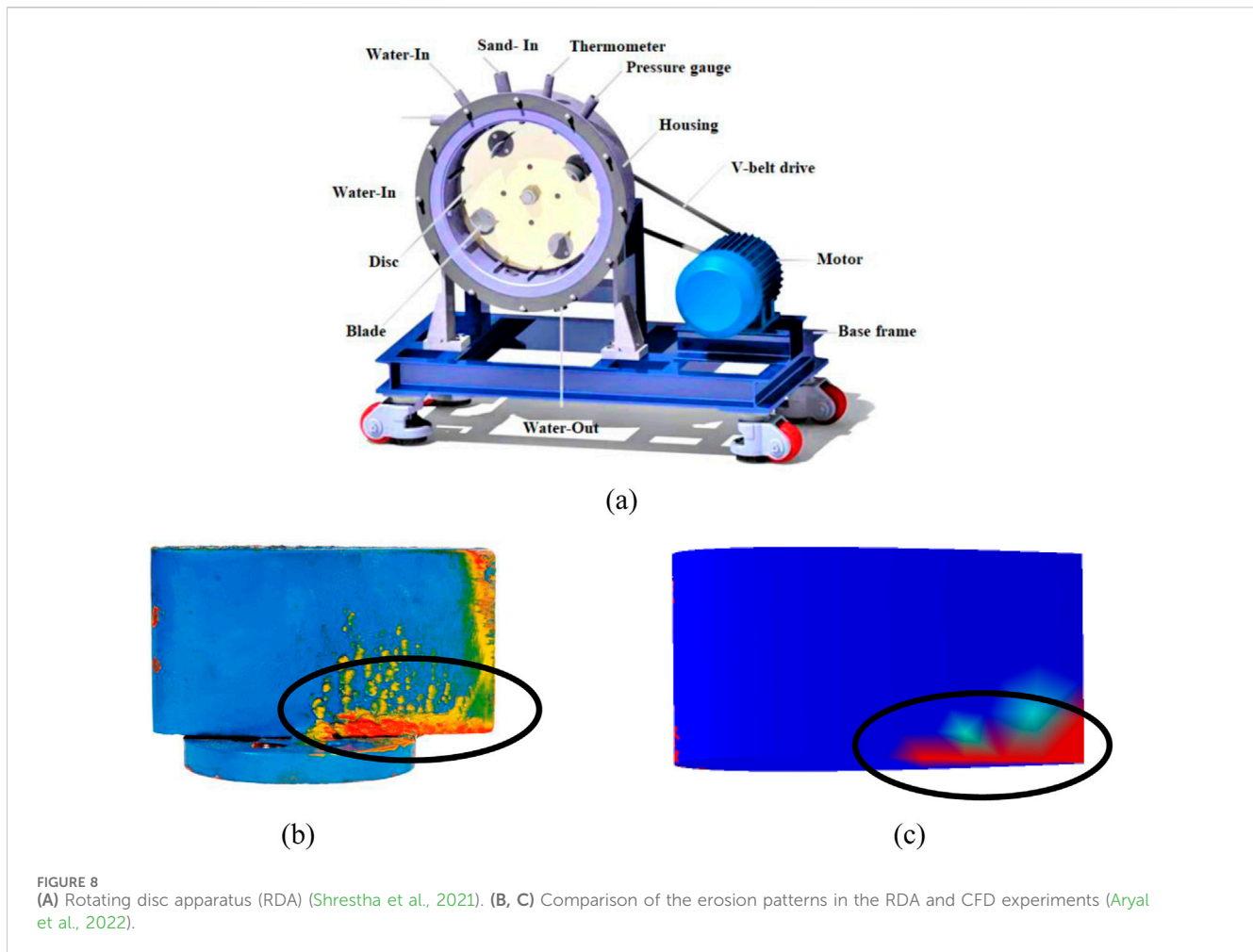


FIGURE 8 (A) Rotating disc apparatus (RDA) (Shrestha et al., 2021). (B, C) Comparison of the erosion patterns in the RDA and CFD experiments (Aryal et al., 2022).

cavitation erosion on metal specimens. The system used a disk and chamber made of stainless steel, an intermediary device for a more compact design, and a frequency inverter for motor control in order to replicate erosion conditions with various periphery velocities for various disk positions. The test was done on cast iron, aluminum, and brass at 4,400 rpm with flow velocities of 36.7 m/s for cast iron and 47.9 m/s for aluminum and brass. The mass loss in the materials was compared to previous studies done by Veerabhadra Rao et al. (1980), Vivekananda (1983), and Zhiye (1983). The mass loss of brass was comparable to the previous studies. However, the mass loss of aluminum and cast iron was very low and was assumed to be due to the oxidation of these materials. Figure 9A, B shows the rotating disk specimens with bubble inducers as pins and through holes to induce cavitation.

3.4 Guide vane cascade rigs

Guide vanes in a Francis turbine are airfoil-shaped vanes used for flow regulation. These components are one of the most severely affected parts in the Francis turbine due to sediment erosion. The guide vane cascade rig consists of a series of guide vanes arranged in a controlled manner to simulate the flow conditions experienced in the actual turbomachinery. The rig allows researchers to investigate

the aerodynamic properties of the guide vanes, including their lift, drag, pressure distribution, and flow swirling capabilities. The working principle of a cascade rig involves the passage of fluid through the cascade of guide vanes that are carefully positioned and aligned to mimic the flow patterns encountered in the Francis turbine. Sensors and measurement devices are placed strategically within the rig to collect data on various parameters such as velocity, pressure, and temperature (Chitrakar et al., 2016; Thapa et al., 2017).

The cascade rig experiments are used to validate CFD models, optimize the design of guide vanes, and understand the fundamental flow phenomena like the leakage flow effect occurring in Francis turbines. Thapa et al. (2016) proposed two alternative designs and optimization for the three-guide vane cascade rig and one-guide vane cascade rig that could replicate the velocity distribution of the turbine of the Jhimruk Hydropower Plant. The study used both analytical and CFD methods along with experimental validations to design and optimize the cascade rig. Supplementary Figure S5 shows the reference turbine layout and the section considered for the three-guide vane cascade from the five chosen guide vanes.

Five guide vanes with four flow channels were taken into consideration for the construction of the reference case guide vane cascade rig, with two outer GV's forming the cascade walls. The walls defined by the free vortex flow profile are taken from the spiral casing center to direct the vane input. Instead of using a

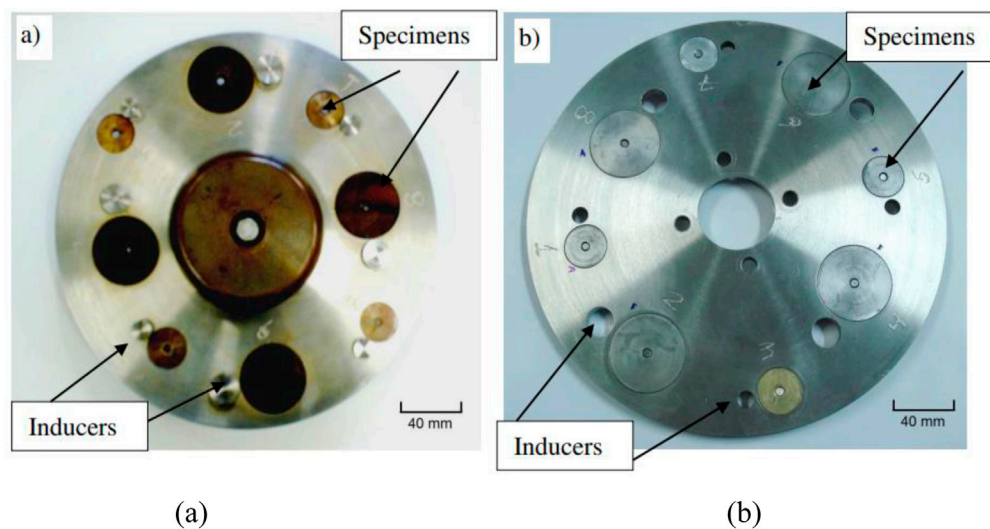


FIGURE 9 Rotating disk specimens with bubble inducers (A) pins and (B) through holes (Divo Bressan et al., 2014).

circular section, the cascade was created using flat plates of the same height. The skewness in the velocity distribution and the optimized design raised the curvature for the inner walls and decreased it for the outside walls to lessen skewness. The velocity distribution across the reference design and optimized cascade rig is shown in [Supplementary Figure S5B](#). The experimental setup of the cascade rig setup to study the particle image velocimetry (PIV) is shown in [Figure 10](#). [Chitrakar \(2018\)](#) considered the three-guide vane cascade rig to test in various GV angles, which could cover 60° of the full guide vanes of the Jhimruk Hydropower Plant. From the experiments in the three-guide vane cascade rig setup, [Koirala et al. \(2019\)](#) found that the erosion at the GV increases the pressure at the GV outlet. The most vulnerable region of the GV was found to be the leading edge, along with the trailing edge and clearance gap.

3.4.1 Particle image velocimetry (PIV)

Particle image velocimetry (PIV) is a technique used to visualize the velocity of fluid particles by capturing the movement of “seed” particles like silica, which are introduced into the flow ([Grant, 1997](#)). These particles are chosen for their ability to scatter light efficiently and their near-neutral buoyancy, and they are tracked using multiple-exposure photography. The recorded positions of these particles at different times help to analyze the fluid’s velocity ([Adrian and Westerweel, 2011](#)). This method is used to characterize the flow after the erosion.

[Thapa et al. \(2016\)](#) used PIV to visualize the velocity distribution in the guide vane cascade rig. Based on the optimized one-guide vane cascade rig, the experimental test rig setup was made for PIV measurements. The flow field at the clearance gap and the mid-span of the GV is shown in [Figure 11A, B](#). The flow field was found to be similar to CFD done in ANSYS CFX v15.0, and the grid was done using the ICEM O-grid method. The pressure values and the velocity around the GV surfaces are shown in [Figure 11C, D](#). At some points, the PIV velocity measurements could be seen as less stable than the analytical velocity, which could be due to the measurements being conducted at low velocity. [Chitrakar et al. \(2017b\)](#) carried out an

experiment using PIV at different NACA profiles to study leakage flow through Clearance gap (CG). NACA4412 showed the least pressure difference compared to the profiles of NACA2412 and NACA0012, due to the leakage flow, although the clearance gap was observed to be less.

Similar to the three-guide vane cascade rig, a one-guide vane cascade rig ([Thapa, 2016](#)) could also produce a constant velocity profile at the runner inlet similar to that of the Francis turbine. The velocity and distribution for the one-guide vane cascade rig showed the pressure difference in a symmetric NACA profile. Another study by [Chitrakar et al. \(2017a\)](#) compared the leakage flow in guide vanes with different hydro profiles using PIV and found that the leakage flow in the NACA4412 profile was 1.31% less than the reference GV used of NACA0012, which causes leakage flow erosion in a Francis turbine.

4.5 Francis turbine test rigs

A Francis turbine test rig is an experimental setup to evaluate the performance of the Francis turbine at many operating conditions. A model of a Francis turbine of a certain hydropower plant is used as an experimental test setup. An investigation of the erosion in the Francis turbine runner and guide vane was done with an RDA because the results of the erosion were very comparable to the numerical simulation and real case. However, the Francis turbine test rig has conditions similar to the real case of a turbine. Quantitative erosion testing on turbine blades can now be performed using a non-recirculating type of sediment erosion test setup ([Kapali, 2021](#)). The components of the test rig are divided into hydro-rig components: main pump, pressure tank, sediment injector, test rig, and hydro-cyclone separator and measuring components, which include a pressure gauge, pressure transducers, electromagnetic flow meter, VFD, and pressure relief valve, as shown in [Figure 12](#). After developing the test rig, the study also evaluated the erosion patterns and rates on the aluminum test

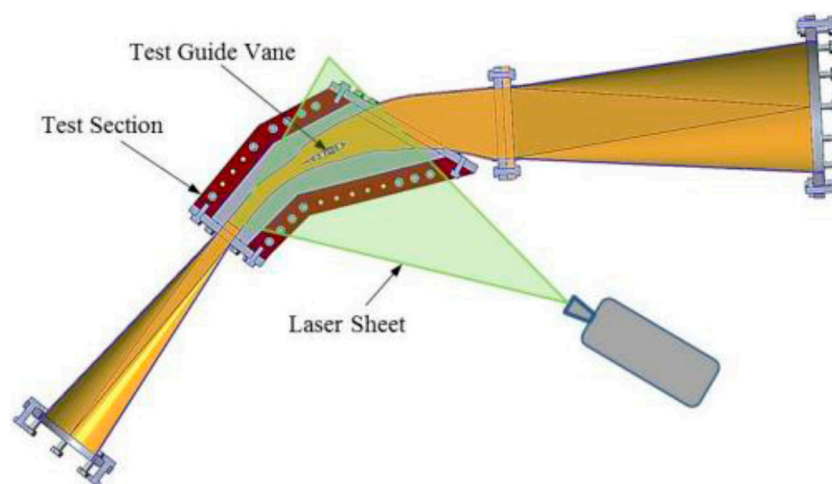


FIGURE 10
One GV cascade rig test setup (Thapa et al., 2016).

blades of the runner by accelerating sediment concentration. The erosion rate was also calculated as the quantity of erosion per unit time of operation as in the Rajkumar model (Rajkarnikar et al., 2013). The average erosion rate was 0.174 mg/gm/hr. The erosion rate prediction seemed to be better than the predicted by the RDA, as the RDA does not consider changes in sediment particle properties after hitting the sample (Noon and Kim, 2021). An experimental study was done to study the performance of the pico-hydraulic Francis turbine using the setup (Kayastha et al., 2020). The study examined the effects of sediments on turbine efficiency. Hydro-cyclone separators reduced the sediments going into the turbine. However, they also cause discharge loss at higher heads.

A study by Poudel et al. (2024) investigated the impact of sediment-laden flow on the performance of Francis turbines. The experiments revealed that sediment presence caused efficiency curves to shift, requiring higher discharge for the same efficiency. While the maximum efficiency remained stable at smaller GV openings, it decreased by approximately 1.1% at larger GV openings. The sediment did not significantly affect the head but slightly reduced output power. These findings signified the importance of sediment management in maintaining the efficiency and durability of Francis turbines, particularly in sediment-rich regions like the Himalayas. The experimental setup used for the study is shown in Figure 13.

3.6 High-velocity test rigs

High-velocity test rigs were developed for testing specimens with varying curvature geometry to replicate the flow hitting a Pelton turbine bucket (Guo et al., 2020). The specimen material was aluminum with varying curvatures. Artificial silica sand (coarse sand) with a size of 256 μm and Baskarp-15 foundry sand (66% free quartz, fine sand) with a size of 174 μm were the erosive particles used. The findings of the study were presented by analyzing the erosion rate for curved specimens. Based on the visual analysis of the degraded particles, it was concluded that the bulk of the coarse

grains felt closer to the splitter, while the fine grains were seen to fall farther from it. Moreover, a decrease in the erosion rate was noted for finer particles, as shown by the weight loss per hitting particle. This was ascribed to the smaller particles' reduced impact energy as well as the potential that some of the finer particles were able to glide without coming into contact with the surface. Another noteworthy observation was that the erosion rate, expressed in milligrams per kilogram, increased as the curved radius of the specimens increased (Ge et al., 2023). Figure 14 depicts the schematic diagram of the high-speed test rig.

The Pelton turbine performance and erosion test equipment was designed to monitor Pelton turbine system performance in real-world hydropower plant scenarios. The test equipment may measure the turbine's sand erosion rate in addition to its performance. The three primary categories of test rig components are hydro-rig components, electrical components, and measuring and controlling devices. Supplementary Figure S6 shows the Pelton turbine erosion test facility. The hydro-rig components include a reservoir tank, pump, surge tank, penstock pipe and feeding unit, turbine, drive system, tail race, and settling basin. The electrical components include an induction generator controller (IGC). The measuring and controlling devices include two pressure gauges (liquid-filled and vacuum), a rotary torque transducer, and an ultrasonic flowmeter (UFM) (Thapa, 2004a). The efficiency loss was correlated with the change in splitter thickness after erosion. The correlation showed that there was a 1% loss in efficiency with a 1-mm change in splitter width. The efficiency of the turbine was also correlated with respect to mass loss only using concentration and operating hours (Bajracharya et al., 2007a).

The effects of various factors on erosion under actual conditions have been investigated experimentally. Brass was used to create erosion quickly in the turbine buckets. Three sides of the tank were encircled by a cooling water jacket to keep the water temperature steady. Correlations between the size and concentration of silt particles and jet velocity, two important parameters, and the wear rate of Pelton turbine buckets have been established based on experiments collected for various parameters (Ge et al., 2023;

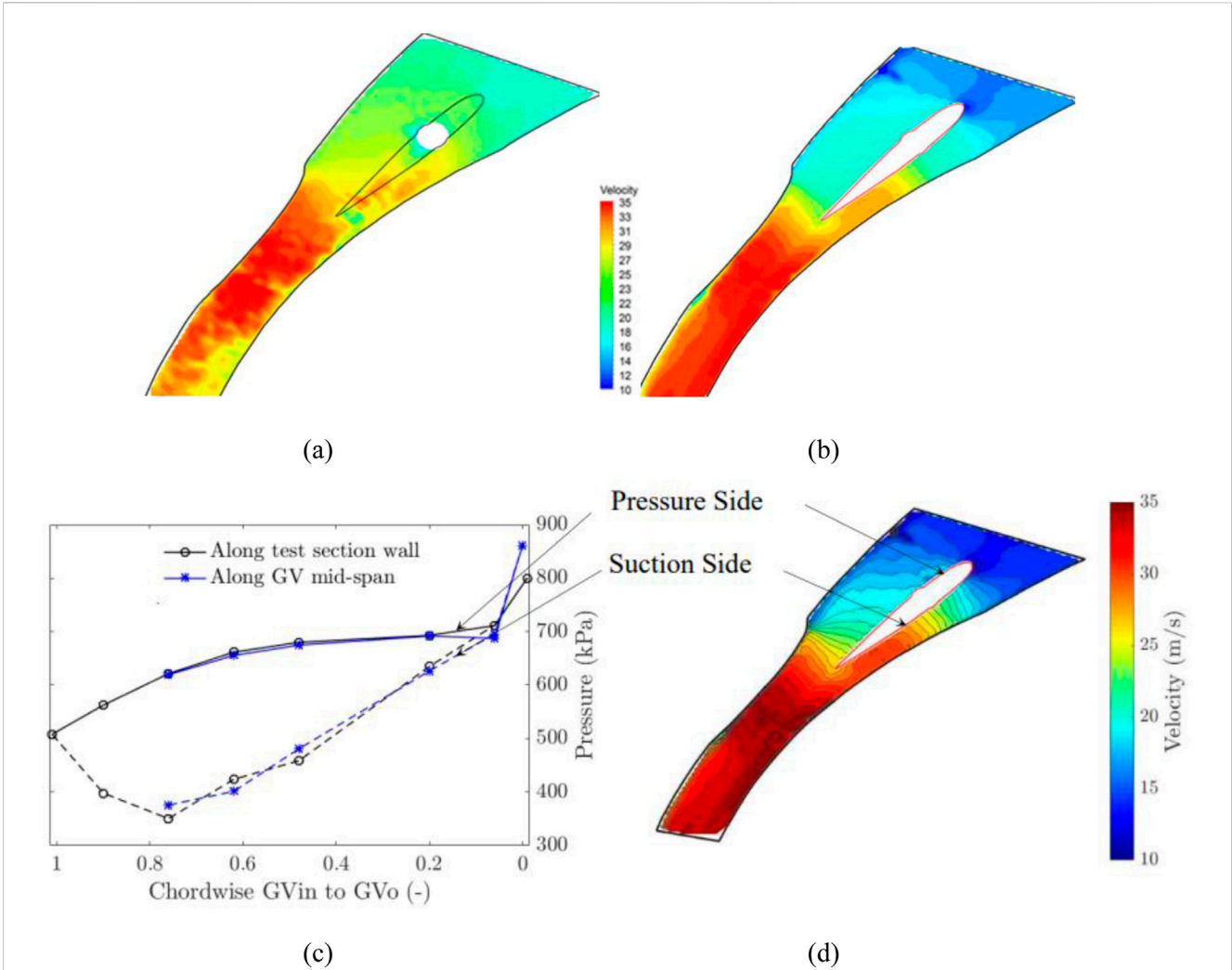


FIGURE 11 Velocity field: (A) Leakage flow at CG, (B) Mid-span of a GV cascade rig (Chitrakar et al., 2017a), (C) Pressure values at GV surfaces, and (D) Velocity field around GVs (Singh Thapa, 2016; Thapa et al., 2018).

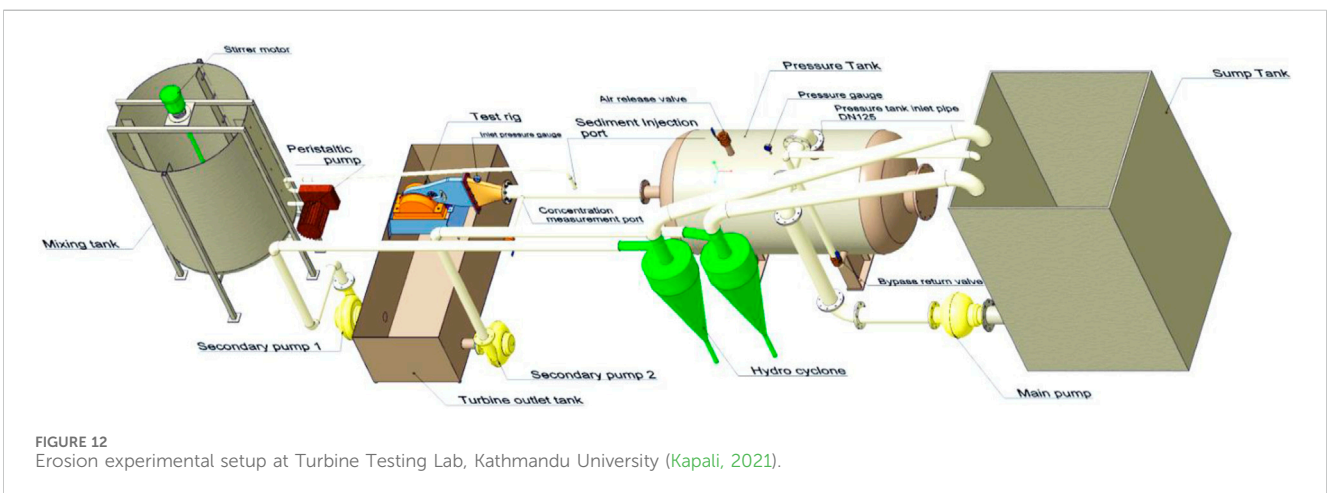
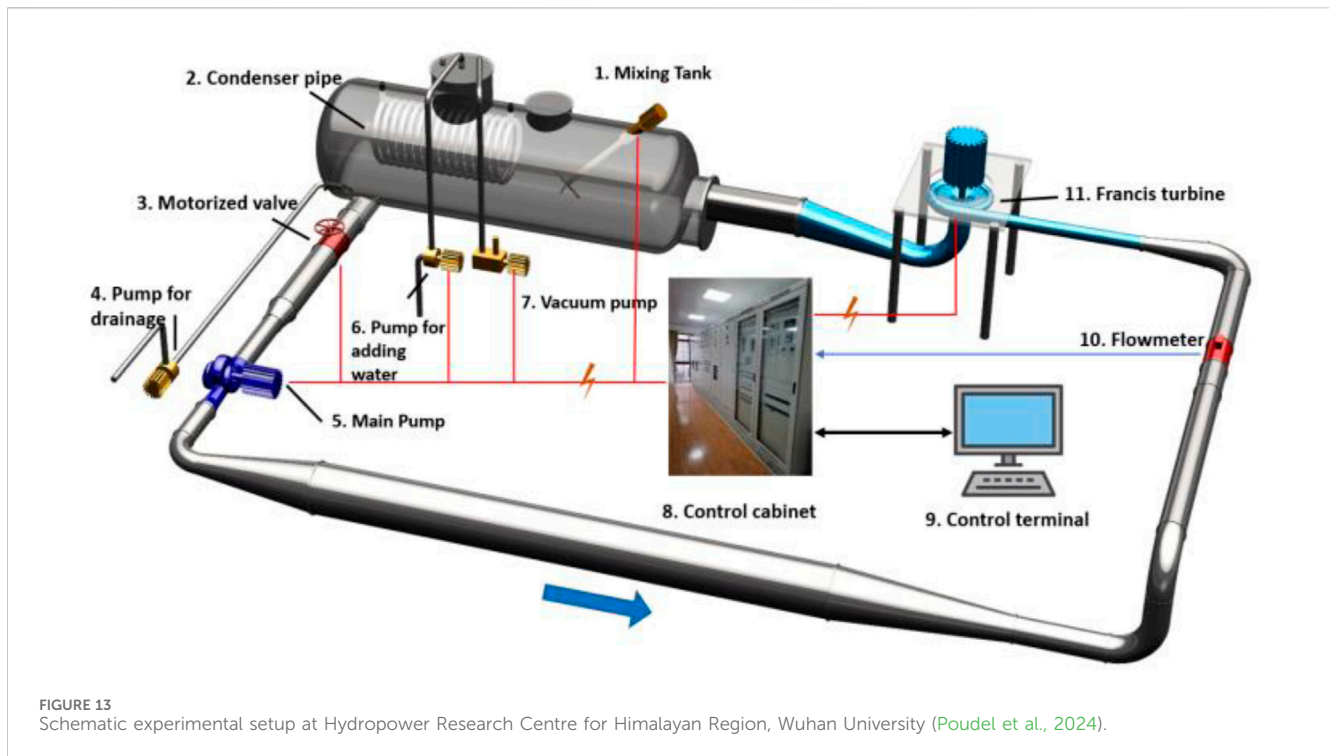


FIGURE 12 Erosion experimental setup at Turbine Testing Lab, Kathmandu University (Kapali, 2021).



Bajracharya et al., 2007). Figure 15 shows the schematic diagram of the Pelton turbine hydro-abrasive test facility.

A consistent rise in the rate of erosive wear with time is indicated by normalized wear, which is defined as weight loss/initial bucket weight and increases approximately linearly with running time. This wear rate fluctuates greatly when comparing different particle sizes and concentrations, yet it stays constant for a given concentration and particle size. The erosive wear rate also increases with higher concentrations, although the rate is not consistent across different size ranges. The normalized erosive wear shows a rising trend as the particle size increases, especially at higher concentrations, especially at 10,000 ppm. This pattern is also shown when comparing the mean particle size (D_{50}) for different concentrations. This finding aligns well with previous studies in the field. Investigating normalized wear per unit discharge versus jet velocity for a fixed size and concentration reveals that the erosive wear rate follows a power law relationship with respect to jet velocity, expressed as $W \propto v^n$. The experimental determination of n yields a value of 3.79, which is consistent with findings from other investigations focused on Pelton turbines (Leguizamón et al., 2019; Padhy and Saini, 2012).

A consistent rise in the rate of erosive wear with time is indicated by normalized wear, which is defined as weight loss/initial bucket weight and increases approximately linearly with running time. This wear rate fluctuates greatly when comparing different particle sizes and concentrations, yet it stays constant for a given concentration and particle size. The erosive wear rate also increases with higher concentrations, although the rate is not consistent across different size ranges. The normalized erosive wear shows a rising trend as the particle size increases, especially at higher concentrations, especially at 10,000 ppm. This pattern is also shown when comparing the mean particle size (D_{50}) for different concentrations. This finding aligns well with previous studies in the field. Investigating normalized wear

per unit discharge versus jet velocity for a fixed size and concentration reveals that the erosive wear rate follows a power law relationship with respect to jet velocity, expressed as $W \propto v^n$. The experimental determination of n yields a value of 3.79, which is consistent with findings from other investigations focused on Pelton turbines (Leguizamón et al., 2019; Padhy and Saini, 2012). Figure 16A–C shows the bucket of the Pelton turbine after the experimentation in the erosion test facility.

Padhy and Saini (2012) studied the impact of Pelton bucket mass loss on turbine output and efficiency. The operating parameters (flow velocity, operating time) and sediment parameters (silt size and concentration) were studied to develop the correlation with efficiency loss using the experimental data. The bucket shape alteration was also responsible for further efficiency loss. The efficiency loss trend shows the initial high rate of efficiency loss with a slowly decreasing trend that became asymptotic over a prolonged period of turbine operation. The study also explored the impact of sediment shape and size on turbine erosion, utilizing experimental and computational analyses. Utilizing fast Fourier transform (FFT), the research identifies particle shapes and numbers that will further help quantify their impact on turbine materials. Digital image processing and regression analysis were used to characterize their effects. Results showed that irregularly shaped particles of smaller size caused higher erosion rates than larger ones of the same shape. The study reveals a gradient of erosion capacity of sediment from upstream to downstream locations, with higher erosion in the higher altitudes and lower erosion in the lower altitudes. The study also noted that abundantly available shapes of sediment have a greater impact. Elongated particles are profuse in rivers and have the highest effect on erosion among all other particle shapes (Poudel et al., 2012). Two main erosion mechanisms are dominant in the erosion of a Pelton turbine: cutting/abrasive and

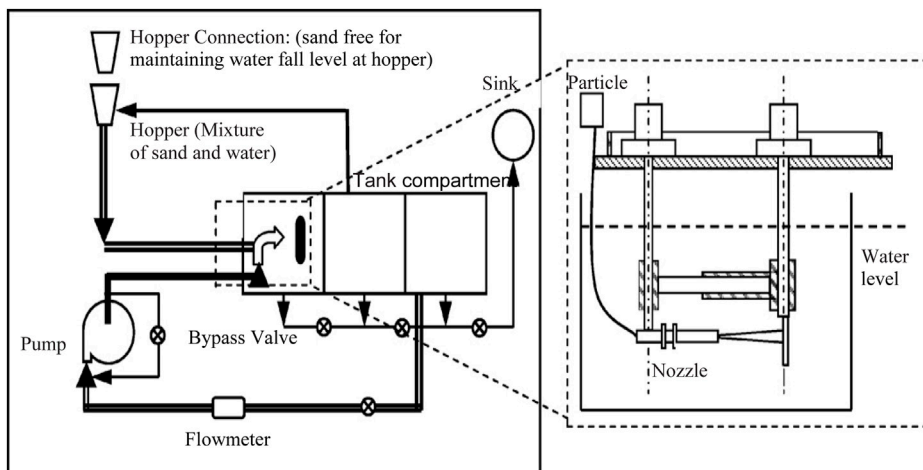


FIGURE 14 Experimental arrangement of high-speed test rig (Thapa, 2004a).

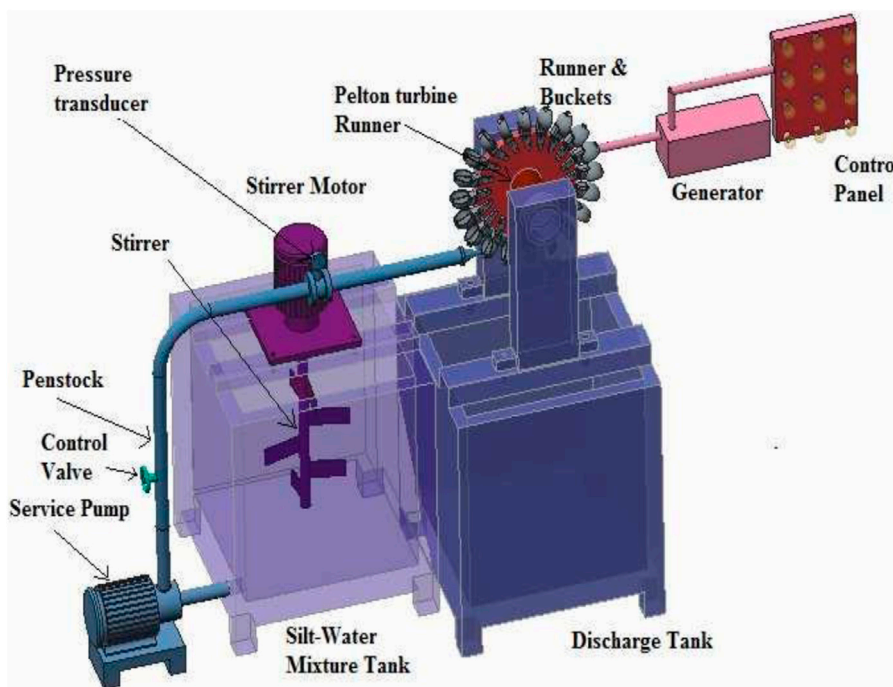
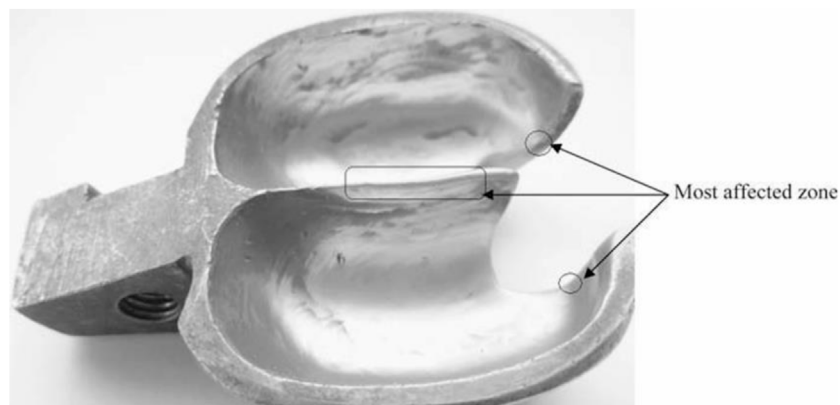


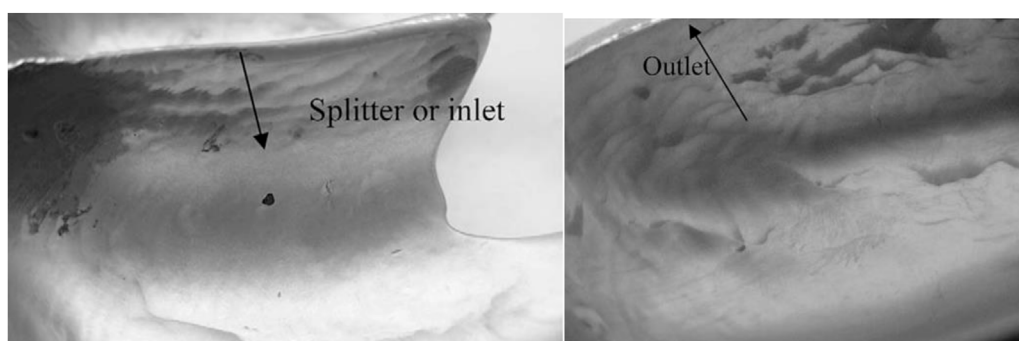
FIGURE 15 Schematic diagram of the Pelton turbine hydro-abrasive test setup (Thakur et al., 2017a).

surface fatigue/erosive wear. The cutting erosion mechanism is dominant for the outlet and splitter vicinity regions. The surface fatigue and plastic deformation erosion mechanism is dominant for the splitter. The erosive wear mechanism is dominant for bucket depth regions (Padhy and Saini, 2012). The bucket depth is the most eroded region. Abgotsson et al. (2013) performed a wear study on the Pelton turbine bucket, splitter, and cutout regions before and after the increment of suspended sediment concentrations during peak seasons. The study showed the importance of accurate measurement and monitoring of two main sediment parameters,

suspended sediment concentration and particle size distribution, to understand how progressive erosion degrades turbine efficiency. The results will be significant for the design, operation, and maintenance optimizations of the reference hydropower. The study performed suspended sediment monitoring (SSM) using different types of monitoring devices that are based on different operating physical principles. The devices are turbidimeters (in-line and submerged), acoustic discharge measurement (ADM), and a laser diffractometer. The turbidimeters had a problem with signal drift due to particles blocking optics. Turbidimeters with self-



(a)



(b)

(c)

FIGURE 16
(A) Pelton bucket surface after experiments, **(B)** magnified view of a splitter, and **(C)** Pelton turbine bucket's outlet edge showing the flow direction (Padhy and Saini, 2009).

cleaning systems or optics that are not in contact with sediment-laden flow (free-falling jet type) are suggested. Laser diffractometers measure both suspended sediment concentration and particle size distribution, and for the flows with variable particle sizes, laser diffractometers measure suspended sediment concentrations more accurately than turbidimeters and ADM devices because these devices are based on particle size-dependent calibration.

3.7 Special test rigs

3.7.1 Integrated test rig

An erosion test system for hydraulic machinery (ETS-HM) was developed by Lu et al. (2014) that was capable of performing an erosion study incorporating the synergetic effect of cavitation and sand erosion. The test system comprises three different test modes, as shown in Supplementary Table S3. The venturi-section water tunnel rig and rotating disk test can measure both the cavitation and sand erosion, whereas the rotating disk with nozzle injector is only capable of measuring the sand abrasion, that is, without cavitation. The test system used programming logic control (PLC) to automatically control the pumps, valves, and sensors. The test system is also composed of high-technology measurements and instrument tools. The eroded sample's weight loss was evaluated using a high-precision analytical electronic balance, and the eroded

volume was calculated by integrating the erosion depth and using a 3D auto surface profiler to produce the eroded surface's shape. The test system provided insights into the estimation of cavitation and sediment erosion in a Francis turbine. The schematic diagram of the integrated coalesced test facility for ETS-HM is shown in Figure 17. Another integrated test rig used for validating the sand erosion models consists of a specialized pipeline setup equipped with an elbow section where multiphase flow can be simulated. It includes mechanisms for controlling and varying flow rates, pressure, and sand concentration. The rig is instrumented with sensors to measure erosion rates and particle velocities, allowing for accurate data collection and analysis (Kang and Liu, 2020).

3.7.2 High-temperature erosion test rig

The high-temperature erosion test rig is a sophisticated apparatus designed to assess the erosive wear of materials under controlled, high-temperature situations. It featured independent temperature control for impact particles, air, and test pieces, allowing precise regulation up to 900°C. The setup included a chamber that prevents oxidation of test pieces, ensuring consistent testing conditions. Particles are heated and accelerated by hot air to impact the test specimens, which can be adjusted to impact angles from 0° to 90°. The design enabled accurate and reproducible measurements of erosion rates, making it particularly effective for evaluating the wear resistance of materials like S50C

steel, SK3, and high V–Cr–Ni stainless spheroidal carbides cast iron (SCI-VCrNi) at elevated temperatures (Shimizu et al., 2009). Figure 18A, B shows the schematic and picture of the high-temperature erosion test rig.

3.7.3 Slurry erosion test loop rig

The slurry erosion test loop rig (Wu et al., 2011) consisted of two primary experimental flow loops designed to simulate different erosion conditions. The slurry flow test loop featured a 3000-L agitated slurry holding tank, a Warman 3 × 2 slurry pump, and an Emerson magnetic flowmeter. It employed silica sand particles with a median diameter of approximately 200 μm, mixed with tap water at a 7% concentration, and recirculated through a pipe with an internal diameter of 53 mm at velocities ranging from 0 to 10 m/s. The air/solids flow test loop, on the other hand, used a Robushi E106 75 kW blower to recirculate sand or glass particles with diameters of 50–500 μm at a maximum velocity of 80 m/s. The test pipe sections in this loop had a minimal diameter of 100 mm. A mixing tank with an agitator was employed to study erosion on rotating impellers, utilizing sands or glass particles with diameters ranging from 100 μm to 200 μm. This setup allowed for comprehensive testing of erosion patterns across different flow regimes and equipment configurations.

4 Erosion models

The erosion models are mathematical equations that show the relationship between erosion rate and influencing factors, and they are developed based on the data collected through controlled experiments. The related parameters are systematically varied in the laboratory setting to observe the corresponding erosion effects. The resulting data are then analyzed using statistical approaches to formulate predictive equations that describe erosion behavior under specific conditions. Erosion is then defined based on mass loss per unit mass of material, mass loss per unit area and time, volume eroded, thickness loss with time, etc. These models are essential tools for erosion prediction of similar turbines with insights into designing, optimizing, and maintaining hydraulic components, ensuring their efficiency, reliability, and longevity. The types of experimental setups vary for the purpose of the study and working principle of the turbines. Most of the previously designed test rigs are based on simplified assumptions and cannot replicate the operating conditions and erosion mechanism occurring in actual hydropower plants. Thus, the current erosion models have not been found to reliably or accurately predict erosion. The subtopics below explain the various erosion models developed based on the types of experimental setups for erosion study on materials and Francis and Pelton turbine components.

4.1 Erosion models based on experiments in jet tester rigs

In a jet tester rig, erosive conditions are introduced by directing a high-speed jet of abrasive particles suspended in fluid at a target material. In this setup, key variables such as particle velocity, particle size, impact angle, and the properties of both the abrasive material

and the target surface can be measured and controlled. Neilson and Gilchrist (1967) used aluminum, glass, and polymer as the base and target materials to study erosion in a jet tester rig. The abrasive particles were alumina in an air jet with angle of attack, particle velocity, and concentration as the control variables. The erosion equation from the experiment with erosion rate being calculated as the mass loss per unit time of abrasive particles impacting the target. Elkholy (1983) conducted an erosion study on cast iron with silica as the erodent in water. The control variables were volume concentration, mass concentration, and diameter of particles, along with angle of attack and particle velocity. The derived erosion equation is calculated as mass per unit mass of abrasive materials, and the equation also depends upon the hardness of base materials and erodent along with the concentration, diameter of particles, angle of attack, and particle velocity. Wiederhorn and Hockey (1983) used five different test materials, namely, sintered alumina, sapphire, silicon, sintered magnesium oxide, and fused silica. Carborundum grains in the air were used as the erodent in the experiment. The control variables in the experiment were the particle concentration, particle velocity, size of the particle, and the impact angle of the jet. The derived equation is in terms of the volume loss of the base material depending upon the toughness, hardness, and brittleness of materials along with the size of the particle and angle of attack of the jet. Turenne et al. (1989) studied the erosion properties of aluminum and glass when exposed to silica in water. The control variable was the concentration of the particles in water. The erosion rate equation is in terms of the weight loss of the base material per unit gram. Haugen et al. (1995) tested alumina, zirconia, yttria zirconia, carborundum, and titanium diboride materials using silica and alumina as erodents and oil and gas as solvents. The control variables in the experiment were the mass of the particle, particle velocity, and the impact angle of the jet. The erosion rate equation was calculated as the weight loss of the base material per unit kilogram. Yan et al. (2020) conducted an experiment on an alpha-beta titanium alloy having a strong specific strength and resistance to corrosion. The erodent used was quartz in an air jet. The control variables in the experiment mainly were the particle concentration, particle velocity, size of the particle, and the jet impact angle. The erosion rate was calculated as milligrams per gram. The details about the tested specimen, erodent, and erosion model equation derived from the experiments are listed in Table 2.

4.2 Erosion models based on experiments in pot tester rigs

The pot tester rig consists of a cylindrical vessel filled with a slurry of abrasive particles and fluid. The speed of the impeller, the concentration of abrasive particles, and the properties of the fluid are controlled to mimic different erosion conditions in a pot tester rig. Tsai et al. (1981) experimented on A-53 mild steel, 304, and 316 stainless steels with coal and carborundum particles as the erodent in kerosene. The resulting equation derived from the experiment gives erosive wear rate per unit area, which depends upon the concentration of eroding particles, diameter of eroding particles, properties of base materials, and velocity of eroding particles. Gupta et al. (1995) studied the erosive properties of

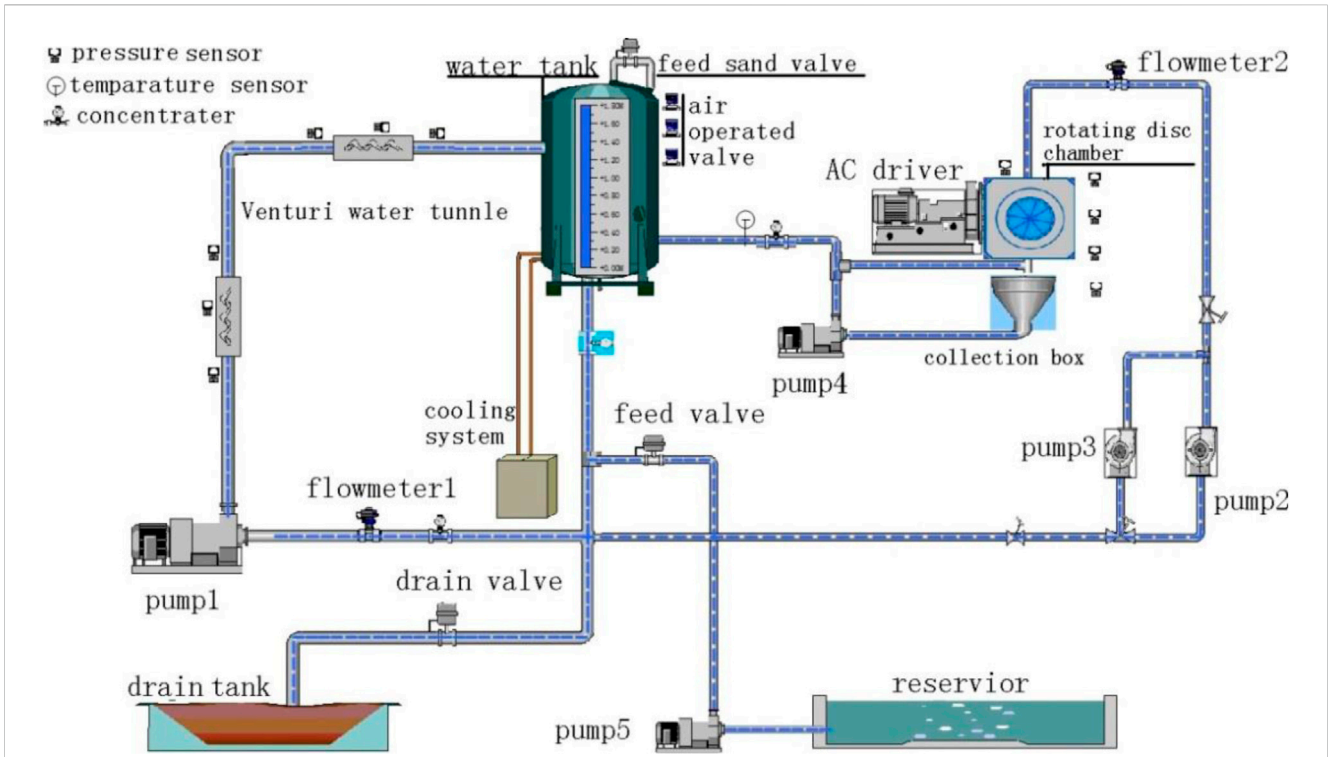


FIGURE 17 Arrangement of an integrated coalesced test facility for ETS-HM (Lu et al., 2014).

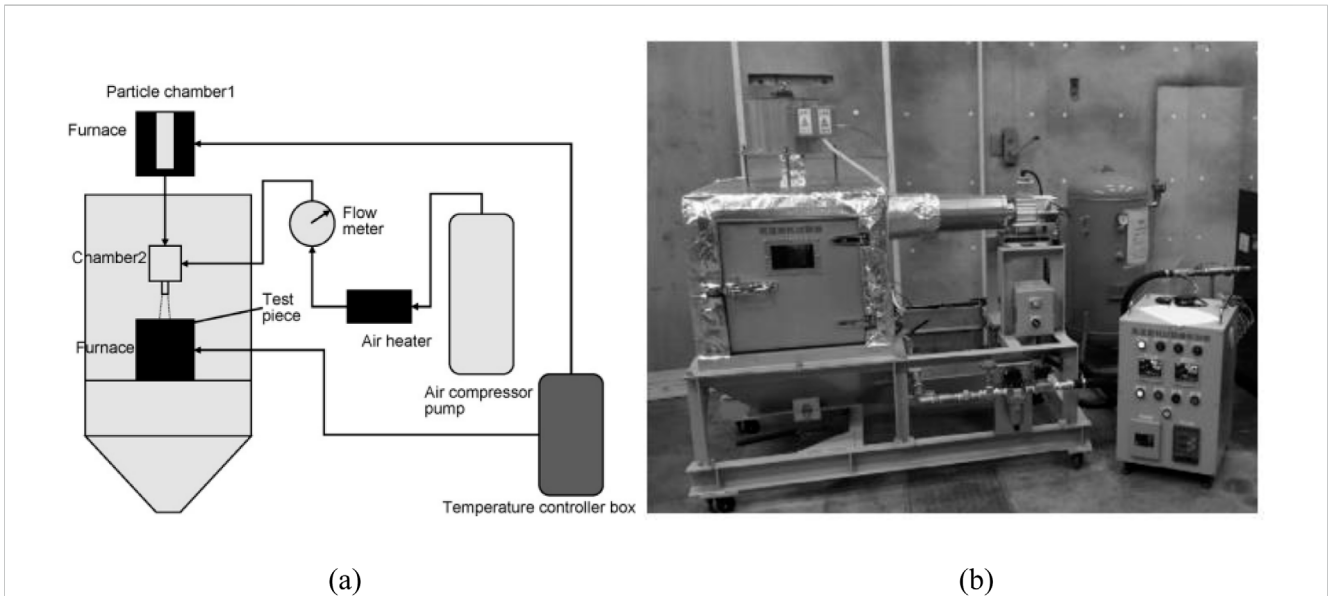


FIGURE 18 (A) Schematic diagram of high-temperature erosion test setup. (B) High-temperature erosion setup (Shimizu et al., 2009).

brass and mild steel when exposed to erosion due to copper in water. The erosion equation for both the materials derived from the experiment gives erosion in terms of erosive wear per unit time, and the wear rate depended on the concentration by weight of particles, particle diameter, and flow velocity. Clark and Wong

(1995) used different materials to test erosion properties with carborundum and aluminum in diesel. The erosion rate equation from the experiment is the sum of cutting erosion and deformation. Patil et al. (2011) subjected silica particles in water to a pot tester rig to study the wear in aluminum. The erosion equation gives the

erosion rate, which depends upon the impact angle along with the concentration by weight of the particles, flow velocity, and diameter of the particle. More et al. (2014) used AISI steel and SS304L as base materials, which were subjected to erosion by quartz and water mixture in a pot tester. The hardness of the erosive particles, flow velocity, impact angle, diameter of the erodent particles, and particle concentration by weight all affect the erosion rate, which is determined by the erosion equation. Tarodiya and Gandhi (2019) used 304L steel, gray cast iron, and high chromium white cast iron as the testing materials. Silica and iron oxide particles in water were used as the mixture in the pot. The erosion rate derived from the experiment depended upon the impact angle, velocity of the impacting particles, and diameter of the particles. The details about the tested specimen, erodent, and erosion model equation derived from the experiments are listed in Table 3.

4.3 Erosion models based on experiments in Francis turbine test rigs

In the Francis turbine test rig, erosion is induced with a test setup similar to that of a hydropower plant. Even though Finnie, Tabakoff, and Grant's erosion model and Oka's erosion model are not derived from the experiments in a Francis turbine test rig, these erosion models have been found to accurately predict the erosion rates in the Francis turbine. Finnie (1960a) conducted experiments on various ductile and brittle materials when exposed to alumina and silicon carbide in air or water. The erosion is predicted in terms of the volume of materials eroded, which depends upon the mass of the particles, flow velocity, impact angle, shape factor, and the diameter of the ring crack. The model described by Grant and Tabakoff (1973) predicted erosion by studying wear in aluminum alloy when exposed to alumina particles in water. The erosion rate equation derived is in terms of the velocity of particles, the angle of impingement, and the angle of maximum erosion. Bardal's erosion model equation describes a general form of erosion equation, which gives erosion in mm/year and depends upon material properties, particle concentration, flow velocity, and impact angle (Bardal, 1985). The Oka erosion model used different materials to predict the wear when subjected to silica and silicon carbide in water and air (Oka et al., 1993). The erosion rate is in terms of particle density, fluid velocity, particle velocity, hardness of particles, and the impact angle. The erosion rate equation derived by Tsuguo (1999) predicted loss of thickness per unit of time, which depends upon turbine coefficient, flow velocity, hardness, shape, and size of the erodent particles. The IEC standard (IEC, 2009) equation to predict erosion depth depends upon flow velocity, particle load, concentration, and material properties. Thapa modeled the erosion rate equation, studying the hydropower with a Francis turbine. The size, shape, and hardness of the abrasive particles all affect the expected erosion rate. The Rajkumar model measured the weight loss following erosion to estimate the erosion rate (Rajkarnikar et al., 2013). The base material subjected to wear was aluminum, with the mixture of sediment particles in water as the erodent. The Nandakumar erosion model (Huang et al., 2008) is based on the Finnie and Bitter erosion models. The experiment was done on three different materials: aluminum, copper, and SAE-1055 steel, using carborundum as the erodent in water. The derived equation depends

upon the total mass of the erodent, the width of deformation due to erosion, the density of the particle, the diameter of the particle, the flow velocity, and the angle of impingement. The details about the tested specimen, erodent, and erosion model equation derived from the experiments are listed in Table 4.

4.4 Erosion models based on experiments in Pelton turbine test rigs

Most of the correlations for the erosion rate of Pelton turbine components were developed with respect to sediment characteristics (size, concentration, and mineral content), operating conditions (jet velocity, impingement angle, and operating hours), and base material properties (hardness and wear resistance coefficient). The authors have also accounted for sediment shape and hardness (Naidu, 1997b; Asthana, 1997; Tsuguo, 1999). In the past, silica sand was used mostly for erosion experiments with an air medium (Finnie, 1960b; Bitter, 1962; Neilson and Gilchrist, 1968; Hutchings, 1981). Brass and bronze were used as the base material for rapid erosion results (Bain and Bonnington, 1970; Naidu, 1997b; Padhy and Saini, 2009). The erosion models were able to predict material erosion but were still not applicable to predicting the erosion of hydraulic components. Later, river sand or quartz was used as sediment with martensitic steels as the base material, which are abundantly used material in hydraulic components. The test rigs simulating the actual condition of the Pelton turbine were developed, providing improved correlation for erosion prediction. Most of the erosion models are developed for bucket erosion. The correlation for efficiency reduction has also been developed using the erosion models (Padhy and Saini, 2009; Bajracharya et al., 2008). Liu et al. (2012) and Liu et al. (2019) have developed erosion correlations for a Pelton injector system: needle, nozzle, and buckets. Currently, erosion models are developed for various types of bucket materials: 13Cr-4Ni, 16Cr-4Ni, 16Cr-5Ni, and coated materials: 13Cr-4Ni with plasma-sprayed Cr₂O₃ coating and 13Cr-4Ni with a WC Co-Cr high-velocity oxygen fuel (HVOF) coating (Rai et al., 2020). The various types of erosion models developed for erosion prediction of Pelton turbine components with parameters and model descriptions are discussed in Table 5.

5 Turbine material wear

The erosion and wear of turbine components are significantly influenced by the material properties of the turbine blades and other surfaces in contact with water. Various studies have emphasized the role of material composition, hardness, and surface roughness in determining the erosion resistance of these components (Nakamoto et al., 1993; Sharma and Gandhi, 2021). Commonly used materials include alloys of stainless steel and carbon steel with composite coatings, each exhibiting distinct wear characteristics under different operational conditions. Sharma and Gandhi (2021) studied wear in CA6NM, which is a version of turbine steel used in Bhilangana Hydropower, using SEM photographs. Experimental studies on another turbine steel, CF8M steel with various HVOF sprayed coatings, have shown that WC-10Co-4Cr coatings significantly

TABLE 4 Summary of erosion models based on experiments in a Francis turbine test rig.

Name	Base material	Erodent and solvent	Erosion model	Description of the model
Finnie (1960a)	Ductile and Brittle Materials	E: Alumina SiC S: Air/Water	Ductile materials $Q = \frac{mV^2}{\rho\psi K} (\sin 2\alpha - \frac{\psi}{K} (\sin \alpha)^2)$ if $\tan \alpha \leq \frac{K}{6}$ $Q = \frac{mV^2}{\rho\psi K} (\frac{K(\cos \alpha)^2}{6})$ if $\tan \alpha \geq \frac{K}{6}$ Brittle materials, $d = (constant) (V \sin \alpha)^{0.4}$	Q is the volume of materials eroded, m ³ . m is the single abrasive grain of mass, kg V is the velocity of the fluid, m/s. d is the diameter of the ring crack, m p is the shape factor ψ is the impact angle of the particle relative to the surface in ° α is the impingement angle in ° K is the erosion constant or coefficient
Grant and Tabakoff (1973) and Kang et al. (2016)	Aluminum alloy	E: Alumina S: Water	$E = f(\gamma) (\frac{V_p}{V_1})^2 (\cos \gamma)^2 [1 - R_T^2] + f(V_{PN})$ $f(\gamma) = [1 + k_2 k_{12} \sin(\gamma \frac{\pi}{\gamma_0})]^2$ $R_T = 1 - \frac{V_p}{V_3} \sin \gamma$ $f(V_{PN}) = (\frac{V_p}{V_3} \sin \gamma)^4$ $k_2 = \{1.0 \text{ if } \gamma \leq 2\gamma_0\}$ $k_2 = \{0.0 \text{ if } \gamma > 2\gamma_0\}$ $V_1 = 1/\sqrt{k_1}$ $V_2 = 1/\sqrt{k_3}$ $V_3 = 1/\sqrt{k_4}$	E is the erosion rate, kg/m ² V _p is the velocity of particles, m/s γ ₀ is the angle of maximum erosion V ₁ is the reference velocity 1, m/s V ₂ is the reference velocity 2, m/s V ₃ is the reference velocity 3, m/s
Bardal (1985)	N/A	E: mixture of many sediments like quartz S: Water	$W = K_{mat} \cdot K_{env} \cdot C \cdot V_p^m$	W is the erosion rate, m/year K _{mat} is the material constant K _{env} is the constant according to the environment, C is the concentration of particles, kgm ⁻³ . f(α) is a function of impingement angle α V _p is the velocity of the particle, m/s. m is the velocity exponent
Oka et al. (1993)	Tool steel Carbon tool steel, iron, copper, aluminum, polymethyl methacrylate, polyvinyl chloride, ABS copolymer, nylon-6	E: SiC, silica S: Water, Air	$E = k \cdot (\frac{\rho_p V^2}{H})^m \cdot (\sin(\theta))^n$	E is the erosion rate, m ³ kg ⁻¹ ρ _p is the particle density, kgm ⁻³ V is the velocity of the fluid, m/s H is the material hardness of the particles, HB θ is the impact angle in °
Tsuguo (1999)	Stainless steel	E: Silica S: Water	$W = \beta \cdot C^x \cdot a^y \cdot k_1 \cdot k_2 \cdot k_3 \cdot V^m$	W is reduction of thickness over time, m/year β is the coefficient of the turbine at the degraded portion V is the relative velocity of flow, m/s The average grain size coefficient, denoted by α, is based on a unit value of 0.05 mm k ₃ is the material's abrasion resistance coefficient, whereas k ₁ and k ₂ are the shape and hardness coefficients of the sand particles
IEC standard IEC (2009)	Steel	E: mixture of sand sediments like quartz and feldspar S: Water	$S = W^3 \cdot PL \cdot K_m \cdot K_f$	S is the abrasive depth, m W is the characteristic velocity, m/s PL is the particle load, which is determined by integrating the particle concentration across time K _m is the material factor K _f is the flow factor
Thapa et al. (2012a)	Steel	E: Quartz, Feldspar S: Water	$E = C \cdot K_{hardness} \cdot K_{shape} \cdot K_m \cdot K_f \cdot a \cdot size^b$ $\eta_r = a \cdot (erosion\ rate)^b$ [%/year]	E is the erosion rate, m/year. k _{size} , k _{shape} , and k _{hardness} are the factors that characterize the relationship between abrasion and the abrasive particle's size, shape, and hardness K _m is the variable that describes how abrasion and the base material's qualities relate to one another K _f is the variable that describes how abrasion and water flow relate to

(Continued on following page)

TABLE 4 (Continued) Summary of erosion models based on experiments in a Francis turbine test rig.

Name	Base material	Erodent and solvent	Erosion model	Description of the model
				each component Empirical constants a and b are termed as a = 351.35, b = 1.4976 for a quartz content of 38% a = 1,199.8, b = 1.8025 for a quartz content of 60% a = 1,482.1, b = 1.8125 for a quartz content of 80%
Nandakumar (Huang et al., 2008) et al	Aluminum Copper SAE-1055 steel	E: SiC S: Water	$ER = \frac{\Delta Q}{m} = D\rho_p^{0.1875}d_p^{0.5}V_0^{2.375}(\cos\theta)^2(\sin\theta)^{0.375}$	ER is the erosion rate, m^3s^{-1} ΔQ is the volume loss, m^3 . m is the total mass of the erodent, kg D is the width of deformation due to erosion, m ρ_p is the density of the particle, $kg\ m^{-3}$. dp is the diameter of the particle, m V_0 is the flow velocity, m/s θ is the angle of impingement °
Rajkarnikar et al. (2013)	Aluminum	E: Sunkoshi sample sediment S: Water	$e_r = \frac{W_i - W_f}{W_i \Delta t} \times 100$	e_r is the erosion rate after the test; that is, W_i is the initial weight of the test specimen in kg, W_f is the weight of the specimen after test j in kg, and Δt is the test duration in s

enhance erosion resistance due to their higher hardness than $Al_2O_3+TiO_2$ coatings, which exhibited lower resistance owing to unmelted particles that caused spalling and higher erosion rates (Kumar Goyal et al., 2012). These coatings demonstrated distinct erosion behaviors, with WC-10Co-4Cr displaying a mixed ductile behavior, while $Al_2O_3+TiO_2$ exhibited brittle erosion behavior.

Considering the wear in turbine materials, statistical processing of the obtained results can lead to better optimization of turbine design and materials. By statistical processing of test data, an optimal selection or protection of turbine materials can be made in order to prevent failures, as well as loss of flow or reduction in efficiency in turbine operation. In addition, by applying appropriate distributions, turbine maintenance can be planned to prevent sudden failures, as well as the procurement of spare parts, which is also important from a safety perspective. A research work (Panic et al., 2023) demonstrates the application of the Weibull distribution to model wear patterns in turbine blades, enabling predictive maintenance scheduling. In addition, given the very useful database obtained during the testing of both turbines on the test rig, it is very important to note that the application of some of the statistical data processing methods can contribute to better optimization and reduction of costs and resources during design. Milojević and Stojanović (2018) used the Taguchi method and artificial neural network (ANN)-based models to analyze the effects of material, load, and sliding speed on wear, and similar approaches can be applied to predict and mitigate erosion in turbines. Gajević et al. (2024) used the Taguchi, GRA, and TOPSIS methods to analyze the characteristics of aluminum. These methods can also be applied to identify optimal operating parameters like load, sliding speed, and material composition, which can help to minimize erosion, adhesive wear, and delamination in turbines. The water flow does not need to have a direct impact on the turbine bearings as they do not come in contact with water, but a

review study done by Dhanola and Garg has shown that a new bearing design could help decrease the wear in turbines (Dhanola and Garg, 2020).

6 Summary and conclusion

The issue of sediment erosion in high-head flows poses significant challenges to the efficiency and longevity of turbines. It has been necessary to study the effects of erosion to predict its effect at the earliest possible stage. The investigation of sediment erosion in turbine materials through diverse experimental test rigs and analytical techniques represents a crucial endeavor in turbine engineering. The use of specialized setups such as the jet erosion test rig, rotating disc apparatus (RDA), guide vane cascade rig, Pelton turbine test rig, and Francis turbine test rig has made studies into erosion phenomena at critical turbine components possible. These experimental platforms have also enabled us to visualize and measure the wear in materials through various analyses of erosion effects. The experimental tests have helped to establish the correlation between many various variables involved in turbine erosion. This study also reveals trends in how experimental studies have evolved over time.

The prediction of erosion wear remains a difficult task influenced by factors ranging from fluid dynamics to material properties and operational conditions. Recently, there have been progresses in the study of erosion and cavitation, such as the coalesced effect erosion system study in which the joint effects of erosion and cavitation could be examined, and Francis and Pelton turbine test rigs in which the test condition could be made similar to the hydropower plants. Future research could include more variables, such as corrosion phenomena in the experimental investigation, to be more realistic and focus on enhancing

TABLE 5 Summary of erosion models based on experiments in a Pelton turbine test rig.

Name	Base material	Erodent and solvent	Erosion model	Description of the model
Finnie (1960b)	Ductile material	E: Silica sand S: Air	Equation 1: if $\alpha \leq 18.5^\circ$ $Q = \frac{MV^2}{8P} (\sin 2\alpha - 3\sin^2 \alpha)$ Equation 2: if $\alpha \geq 18.5^\circ$ $Q = \frac{MV^2}{24P} (\cos^2 \alpha)$	Erosion equation for ductile materials Q is the material eroded, m ³ M is the mass of the impacting particles, kg V is the velocity of particles, m/s α is the impingement angle, ° P is the plastic flow stress, which is the continuous horizontal pressure between the substrate and the particles, Pa
Bitter (1962)	Steel	E: Silica sand S: Air	$\epsilon_{VT} = \epsilon_{VD} + \epsilon_{VC}$ $\epsilon_{VD} = \frac{1}{2} \frac{M(V\sin\alpha - K)^2}{\delta}$ For $\alpha \geq \alpha_{p0}$ $\epsilon_{VC1} = \frac{2MC(V\sin\alpha - k)^2}{\sqrt{V\sin\alpha}} (V\cos\alpha - \frac{CV\sin\alpha - K^2}{\sqrt{V\sin\alpha}} x)$ For $\alpha \leq \alpha_{p0}$ $\epsilon_{VC2} = \frac{1}{2} \frac{M[V^2 \cos^2 \alpha - K_1 (V\sin\alpha - K)^2]}{x}$ $C = \frac{0.288}{\gamma} \sqrt{\frac{\rho_p}{\gamma}}$	Total erosion rate (ϵ_{VT}) is the effect of deformation wear (ϵ_{VD}) and cutting wear (ϵ_{VC}) where M is the mass of impacting particles, kg V is the velocity of particles m/s α is the impingement angle of the particles, ° K is a threshold velocity below which no significant erosion occurs due to deformation, m/s δ is a material parameter representing the material's resistance to deformation wear For cutting wear: α_{p0} is a critical angle where cutting wear behavior changes, ° C is a coefficient related to the material and particle characteristics. x is a constant related to the particle and material properties α is the critical angle where cutting wear behavior changes, ° K1 is the material-dependent constant for lower impingement angles ρ_p is the density of the particles, kg.m ⁻³ . γ is the material parameter related to yield strength or hardness, HB
Neilson and Gilchrist (1968)	Mild steel	E: Silica Sand S: Air	Deformation factor (ϵ) = $z^{\frac{1}{4}} \frac{W_d}{\frac{1}{2}M\delta V \sin\gamma - kp^2}$	where ϵ is a dimensionless parameter that represents the intensity of deformation wear based on the experimental conditions $z^{1/4}$ indicates how the deformation factor scales with particle size W_d is the deformation work done by abrasive particles per unit volume, J m ⁻³ M is the mass of the abrasive particles, kg δ is a material-specific constant associated with the base material's ability to withstand deformation V is the velocity of impacting particles, m/s γ is particle impact angle, ° $\sin(\gamma)$ is the impact angle measured with respect to the surface normal, ° k is a constant related to the material's hardness and the efficiency of the erosion process p is a parameter related to the particle size or the concentration of particles
Bain and Bonnington (1970)	Brass	E: Quartz S: Air	$W = KV^\beta d^\gamma C^\phi$	W is the erosion rate, m ² /s V is the velocity of the particle, m/s d is the size of the particle, m C is the solid concentration, kg m ⁻³ The constants K, β , γ , and ϕ are

(Continued on following page)

TABLE 5 (Continued) Summary of erosion models based on experiments in a Pelton turbine test rig.

Name	Base material	Erodent and solvent	Erosion model	Description of the model
				determined by the characteristics of the base material and the erodent
Hutchings (1981)	Mild steel, Mild Steel Alloys	E: Silica Sand S: Air	$\Delta\epsilon_p N_f^{\frac{1}{2}} = \epsilon_c$ $E = \frac{\alpha\sigma^{\frac{1}{2}}V^3}{\epsilon_c^2 H^{\frac{1}{2}}}$	$\Delta\epsilon_p$ is the average strain per impact N_f is for the average number of hits (or strain increments) required to produce material separation E is the mass loss of the target per impinging particle mass unit, kg α is the ratio of the crater's volume to the volume of the plastic deformation in the metal subsurface ρ is the density of the target material, kg m^{-3} σ is the density of the particles, kg m^{-3} H is the dynamic hardness of the target material, HB.
Bardal (1994)	Stainless steel	E: Silica sand, Quartz S: Air	$W = K_{\text{mat}} * K_{\text{env}} * c * V^n * f(\alpha)$	General erosion model for pure erosion W is the erosion rate (material loss) in m/yr K_{mat} is the material constant K_{env} is the constant function of the environment C is the concentration of particles, kgm^{-3} $f(a)$ varies according to the impingement angle α° V is the velocity of the particle, m/s n is the velocity exponent
Krause and Grein (1996)	X5CrNi13/4	E: Quartz S: water	$\delta = \rho q c v^{3.4} f(d_{p50})$	d is the rate of abrasion on a steel Pelton runner (m/h) p is a constant q is the quantity of quartz c is the average sand concentration, kgm^{-3} v is the relative jet velocity, m/s $f(d_{p50})$ is a function defining particle size
Naidu (1997b)	Various metals: Stainless steel, Bronze	E: Silica sand, Quartz S: Water	$W = S_1 S_2 S_3 S_4 M_r v^x$ For the velocity exponent x , $x = \left\{ \begin{array}{l} 3 \text{ for Francis runner} \\ 2.5 \text{ for guide vanes pivot ring liner} \\ 2.5 \text{ for Pelton nozzle} \\ 1.5 \text{ for Pelton runner buckets} \end{array} \right\}$	S_1 is the concentration of the silt coefficient S_2 is the silt hardness coefficient, HB. S_3 is the silt particle size coefficient, m S_4 is the silt particle shape coefficient M_r is the coefficient of the base material's resistance to wear V is the relative velocity of water, m/s X is the velocity exponent
Asthana (1997)	13Cr4Ni Steel	E: Silica sand S: Water	Turbine abrasion (TA) $TA = f(PE, v^2)$ Modified sediment content (PE) $PE = P^\alpha a^\beta K_1 K_2 K_3$ $\alpha = 1$, for concentrations up to 5 g/l $\beta = 1$ for particle size up to 0.6 mm $K_1 = \left\{ \begin{array}{l} 0.75 \\ 1 \text{ depending on irregularities} \\ 1.25 \\ \text{ranging from few to severe} \end{array} \right\}$ $K_2 = \left\{ \begin{array}{l} 1 \text{ for hardness greater than 3 mohs} \\ 0.5 \text{ for hardness less than 3 mohs} \end{array} \right\}$ So, $K_2 = 1$ for 13Cr4Ni steel	PE is the modified sediment content V is the relative speed of the water passing through the turbine sections that have significant abrasion, m/s . z is the exponent of relative velocity P is the average amount of suspended sediment in kgm^{-3} per year α is the correction factor for the concentration of suspended sediment and is the exponent of P . a is the suspended sediment's grain size coefficient with a base of 0.05 mm β is the exponent of a correction factor that represents the average particle size The coefficients K_1 , K_2 , and K_3 are used to adjust the shape, hardness, and abrasion resistance of the base material

(Continued on following page)

TABLE 5 (Continued) Summary of erosion models based on experiments in a Pelton turbine test rig.

Name	Base material	Erodent and solvent	Erosion model	Description of the model
Tsuguo (1999)	Carbon Steel, Stainless Steel	E: Silica Sand, Quartz S: Water	$W = \lambda * c^x * a^y * k_1 * k_2 * k_3 * v_{Char}^z$ $z \geq \{1.5\}$	Rate of erosion measured as the gradual loss of thickness λ is the turbine coefficient in the area of erosion C is the concentration of suspended sediment, $kg\ m^{-3}$ V is the characteristic velocity m/s a is a grain size coefficient average based on unit value for 0.05 mm k_1 and k_2 are sand particle form and hardness coefficients, and the material's abrasion-resistant coefficient, k_3 x , y , and z represent the concentration, size coefficient, and velocity exponent values, respectively
Ratna Bajracharya et al. (2007a)	N/A	E: Quartz S: water	$EM_{flow} = K_2 * F^a * O^{-b}$ where $k_2 = 0.00883456521980509$ $a = 2.1, 4310044472706$ $b = 0.319231938953136$ $Eff_{wl1} = K_3 * M^{-a}$ where $k = 0.7178400502988$ $a = 0.00500250124054351$ $Eff_{wl2} = K_3 (K_{avg} + a_{avg} * C + b_{avg} * O)^{-0.00500250124054351}$ where $k_3 = 0.717840050298804$ $K_{avg} = 38.7550157$ $a_{avg} = 0.004804428$ $b_{avg} = 0.171122597$ $Eff_{wl3} = K_4 * C^{-a} * O^{-b}$ Where $k_4 = 0.71532869$ $a = 0.001373259$ $b = 0.001921144$	EM_{flow} is a mass loss erosion model developed for Pelton turbine buckets F is the flow, m^3/s O is the operating hours, h Eff_{wl1} is the predicted efficiency reduction with respect to mass loss K_n , a , and b are empirical constants based on experiment Eff_{wl2} is the predicted efficiency w.r.t modified mass loss. (The concept of mass loss is dependent on operating hours and concentration.) K_{avg} is the intercept of the model. a_{avg} is the mean of each bucket's concentration elasticity b_{avg} is the mean of each bucket operation hour elasticity Eff_{wl3} is the predicted efficiency w.r.t concentration and operating hours
Bajracharya et al. (2008)	13Cr4Ni	E: Quartz, feldspar, Muscovite, biotite, and others S: Water	Erosive wear rate $\propto a (size)^b$ Where $a = 351.35$ and $b = 1.4976$, for quartz content of 38%, $a = 1,199.8$ and $b = 1.8025$, for quartz content of 60% $a = 1,482.1$ and $b = 1.8125$, for quartz content of 80% Efficiency reduction $\propto a (erosion\ rate)^b$ Where $a = 0.1522$ $b = 1.6946$	Erosive wear rate is the normalized wear rate: a is a coefficient that scales the erosive wear rate based on the particle size and quartz content b is an exponent describing how the erosive wear rate changes with particle size a and b are constants that vary based on the quartz content For efficiency reduction: a coefficient scales the relationship between erosion rate and efficiency reduction b exponent describes the sensitivity of efficiency reduction to changes in the erosion rate
Boes (2009)	CrNi 13/4 steel	E: Quartz S: Water	For $C \leq 45\ mg/L$ $W = 7.56 * 10^{-8} * u^3 * C$ For $C > 45\ mg/L$ $W = 1.82 * 10^{-8} * U^3 * C^{1.375}$	W is the rate of erosion in m^3/sec U is the relative flow velocity, m/s C is the suspended sediment concentration in $kg\ m^{-3}$
Padhy and Saini (2009)	Brass	90% Quartz content sand and water	$W = 4.02 * 10^{-12} * S^{0.0567} * C^{1.2267} * V^{3.79} * t$ $\eta\% = 2.43 * 10^{-10} * t^{0.75} * S^{0.099} * C^{0.93} * V$	W is the normalized erosive wear rate for Pelton turbine buckets $\eta\%$ is the percentage efficiency reduction S is the silt size, m C is the silt concentration, $kg\ m^{-3}$ V is the water jet velocity, m/s . t is the operating hours of the turbine, h Pelton turbine ● Pitch circle diameter = 0.144 m

(Continued on following page)

TABLE 5 (Continued) Summary of erosion models based on experiments in a Pelton turbine test rig.

Name	Base material	Erodent and solvent	Erosion model	Description of the model
				<ul style="list-style-type: none"> No of buckets = 16 Mass of bucket = 0.210 kg Nozzle diameter = 0.010 m Tank dimension $0.6 \times 0.51 \times 0.780 \text{ m}^3$ Centrifugal pump <ul style="list-style-type: none"> Discharge = $0.008 \text{ m}^3/\text{s}$ Rated head = 50 m Penstock pipe <ul style="list-style-type: none"> Outer diameter = 0.060 m Thickness = 0.004 m Sediment test parameters Concentration = 5,000–10,000 ppm Size = 90–335 μm Velocity = 26.61–29.75 m/s T = 8 h
Liu et al. (2012)	Nozzle tip: ZG230-450 Needle shaft 42CrMo Runner bucket X3CrNiMo13-4	E: River sand S: Water	Nozzle tip $E = 5.45 \times 10^{-9} \times V^{3.16} \times C^{0.98}$ Needle shaft $E = 1.47 \times 10^{-9} \times V^{3.41} \times C^{1.02}$ Runner bucket $E = 8.82 \times 10^{-10} \times V^{3.51} \times C^{1.01}$	E is the erosion rate in kg/h C is the sediment concentration, kg m^{-3} V is the resultant flow velocity, m/s
Thakur et al. (2017b)	Aluminum	E: Quartz S: Water	$W = 3.733 \times 10^{-11} \times S^{0.1159} \times C^{0.9096} \times V^{2.285} \times t^{1.1317}$	W is the normalized erosive wear rate S is the silt size, m C is the silt concentration, kg m^{-3} V is the water jet velocity m/s t is the operating hours of the turbine h (standardized wear with $\pm 12.8\%$ error)
Liu et al. (2019)	Runner bucket: (04Cr13Ni5Mo) Needle tip: (ADB610) Nozzle ring: (42ZG230-450)	E: River sand S: Water	Needle tip $E = 5.32 \times 10^{-9} \times W^{4.28} \times C_s^{0.95}$ Nozzle ring $E = 1.07 \times 10^{-8} \times W^{4.07} \times C_s^{1.06}$ Runner bucket $E = 3.45 \times 10^{-9} \times W^{4.31} \times C_s^{1.05}$	E is the erosion rate, m/h W is the resultant velocity, m/s C_s is the sediment concentration, kg m^{-3}
Rai et al. (2020)	Bronze, 13Cr-4Ni, 16Cr-4Ni, 16Cr-5Ni 13Cr-4Ni with plasma sprayed Cr2O3 coating, 13Cr-4Ni with WC Co-Cr HVOF coating	E: Sand S: Water	General Equation $(E_n)_{BGi} = K \times (\text{SSC})^a \times (d_{50})^b \times (V)^c \times (t)^d$ Bucket (Bronze) $(E_n)_{BGi} = 5.74 \times 10^{-12} \times (\text{SSC})^{1.03} \times (d_{50})^{-0.085} \times (C)^{3.10} \times (t)^{1.09}$ Bucket (16Cr-5Ni) $(E_n)_{BGi} = 9.09 \times 10^{-13} \times (\text{SSC})^{1.09} \times (d_{50})^{-0.004} \times (C)^{3.36} \times (t)^{1.11}$ Bucket (16Cr-4Ni) $(E_n)_{BGi} = 7.02 \times 10^{-13} \times (\text{SSC})^{1.08} \times (d_{50})^{-0.0009} \times (C)^{3.42} \times (t)^{1.12}$ Bucket (13Cr-4Ni) $(E_n)_{BGi} = 6.25 \times 10^{-13} \times (\text{SSC})^{1.08} \times (d_{50}) \times (C)^{3.42} \times (t)^{1.11}$ Bucket (13Cr-4Ni with plasma sprayed Cr2O3 coating) $(E_n)_{BGi} = 7.14 \times 10^{-12} \times (\text{SSC})^{1.25} \times (d_{50})^{0.376} \times (C)^{2.42} \times (t)^{1.18}$ Bucket (13Cr-4Ni with WC Co-Cr HVOF coating) $(E_n)_{BGi} = 1.38 \times 10^{-14} \times (\text{SSC})^{1.12} \times (d_{50})^{0.314} \times (C)^{4.09} \times (t)^{0.96}$	Erosion weight loss of Pelton bucket: $(E_n)_{BGi}$ is the bucket's normalized erosion in gm, and SSC is the silt concentration in ppm d_{50} is the median sediment size in mm for a particle size distribution C is the relative flow velocity in m/s. t is the period of time that erosion occurs, h

erosion models through comprehensive validation against experimental data and CFD for exploring advanced materials with enhanced erosion resistance properties. In addition, future research in turbine wear could also include statistical analysis such as Taguchi and TOPSIS methods to analyze the wear in turbine materials. The relationships between turbine wear and turbine bearings could be studied. This approach could be instrumental in minimizing turbine downtime, optimizing maintenance strategies, and ensuring the sustainable operation of hydroelectric power plants. This review combines the findings from a spectrum of

experimental investigations and analytical approaches, providing a resource for advancing turbine technology and mitigating the effects of sediment erosion on turbine performance and durability, ultimately reducing maintenance costs.

Author contributions

RS: data curation, formal analysis, investigation, methodology, writing—original draft, and writing—review and editing. PG: data

curation, formal analysis, investigation, methodology, writing–original draft, and writing–review and editing. SC: conceptualization, methodology, project administration, resources, supervision, validation, writing–original draft, and writing–review and editing. BT: conceptualization, funding acquisition, project administration, supervision, validation, and writing–review and editing. HN: conceptualization, funding acquisition, project administration, resources, supervision, validation, and writing–review and editing. ZG: conceptualization, funding acquisition, project administration, resources, supervision, validation, and writing–review and editing. ZQ: funding acquisition, project administration, resources, supervision, and writing–review and editing.

Funding

The author(s) declare that financial support was received for the research, authorship, and/or publication of this article. This study was performed jointly at the Turbine Testing Lab, Kathmandu University, and the State Key Laboratory of Water Resources Engineering and Management, Wuhan University. The project was supported by the Visiting Scholar's Fund provided by WRHES, China (Project No. 2021SDG01), the EnergizeNepal project (TTL-Energize and ENEP-RENP-II-23-03), and the Hydro Himalaya (NORHED-II) Project.

References

- Abgottspon, A., Staubli, T., Felix, D., Albayrak, I., and Boes, R. M. (2013). Hydro-abrasive erosion of pelton buckets and suspended sediment monitoring. Available at: <https://www.researchgate.net/publication/291339891>.
- Acharya, N., Gautam, S., Chitrakar, S., and Dahlhaug, O. G. (2022). Development of simplified model for prediction of sediment induced erosion in Francis turbine's sidewall gaps. *IOP Conf. Ser. Earth Environ. Sci.* 1037, 012016. doi:10.1088/1755-1315/1037/1/012016
- Adrian, R. J., and Westerweel, J. (2011). *Particle image Velocimetry*. Cambridge: Cambridge University Press.
- Aryal, S., Chitrakar, S., Shrestha, R., and Jha, A. K. (2022). Credibility of Rotating Disc Apparatus for investigating sediment erosion in guide vanes of Francis turbines. *IOP Conf. Ser. Earth Environ. Sci.* 1037, 012034. doi:10.1088/1755-1315/1037/1/012034
- Aslam Noon, A., and Kim, M. H. (2017). Erosion wear on Francis turbine components due to sediment flow. *Wear* 378–379, 126–135. doi:10.1016/j.wear.2017.02.040
- Asthana, B. N. (1997). "Determination of optimal sediment size to be excluded for run-of-river project—a case study," in *Seminar on: silting problems in hydro power stations* (New Delhi, India, Roorkee: WRDTC).
- Bain, A., and Bonnington, S. T. (1970). *The hydraulic transport of solids by pipeline*. 1st ed. Oxford: Pergamon Press.
- Bajracharya, T. R., Shrestha, R., and Timilsina, A. (2019). A methodology for modelling of steady state flow in pelton turbine injectors. *J. Inst. Eng.* 15, 246–255. doi:10.3126/jie.v15i2.27674
- Bajracharya, T. R., Poudel, S., Joshi, C. B., Saini, R. P., and Dahlhaug, O. G. (2007). Correlation between sand led erosion of pelton buckets and efficiency losses in high head hydropower schemes. Available at: <https://www.researchgate.net/publication/296195175>.
- Bajracharya, T. R., Acharya, B., Joshi, C. B., Saini, R. P., and Dahlhaug, O. G. (2008). Sand erosion of Pelton turbine nozzles and buckets: a case study of Chilime Hydropower Plant. *Wear* 264 (3–4), 177–184. doi:10.1016/j.wear.2007.02.021
- Bajracharya, T. R., Pachhain, A. K., Sapkota, A., and Timilsina, A. B. (2020). International Research Journal of Modernization in Engineering Technology and Science 2 (7). Available at: www.ijmets.com.
- Bajracharya, T., Poudel, S., Joshi, C. B., Saini, R. P., and Dahlhaug, O. G. (2008). *Correlation study on sand led erosion of buckets and efficiency losses in high head power plants*. Vienna. Available at: <https://www.researchgate.net/publication/298768075>.
- Bajracharya, T. R., Sapkota, D., Thapa, R., Poudel, S., Joshi, C. B., Saini, R. P., et al. (2006). "Correlation study on sand led erosion of buckets and efficiency losses in high head power plants," in *Proceedings of First National Conference on Renewable Energy Technology for Rural Development 12-14th October Kathmandu, Nepal*.
- Bansal, Dr. R. K. (2010). *A textbook of fluid mechanics and hydraulic machines*. Delhi: Laxmi Publications Pvt. Ltd.
- Bardal, E., Korrosjon og korrosjonsvern. 1985.
- Bardal, E., Corrosion and corrosion protection. 1994.
- Bazanani, G., Bressan, J. D., Klemz, M. A., Tenente, R., and Joao, A. (2008). *Cavitation erosion wear of metallic specimens using the new compact rotating disk device*.
- Bitter, J. G. A. (1962). A study of erosion phenomena. *Wear* 6, 169–190. doi:10.1016/0043-1648(63)90073-5
- Boes, R. M., Real-time monitoring of suspended sediment concentration and particle size distribution in the headwater way of a high-head hydropower plant. 2009.
- Brekke, H. (2002). *Abrasive erosion and corrosion of hydraulic machinery*. London: Imperial College Press.
- Brekke, H. (2002). "Design of hydraulic machinery working in sand laden water," in *Abrasive erosion and corrosion of hydraulic machinery, vol. 2*. Editors C. G. Duan and V. Y. Karelin (London: Imperial College Press), 155–181.
- Burstein, G. T., and Sasaki, K. (2000). Effect of impact angle on the slurry erosion-corrosion of 304L stainless steel. Available at: www.elsevier.com/locate/wear.
- Burwell, J.Jr. (1957). *Survey of possible wear mechanisms*. 2nd ed. New York, NY: Wear 1 (2), 119–141. doi:10.1016/0043-1648(57)90005-4
- Chhetry, B., and Rana, K. (2015). *Effect of sand erosion on turbine components: a case study of kali gandaki 'A' hydroelectric project (144 MW), Nepal*.
- Chitrakar, S. (2018). "Secondary flow and sediment erosion in francis turbines," Doctoral Thesis (Trondheim: Norwegian University of Science and Technology).
- Chitrakar, S., Neopane, H. P., and Dahlhaug, O. G. (2016). "Study of the simultaneous effects of secondary flow and sediment erosion," in *Francis turbines* (Elsevier Ltd.). doi:10.1016/j.renene.2016.06.007
- Chitrakar, S., Neopane, H. P., and Dahlhaug, O. G. (2017b). Particle image velocimetry investigation of the leakage flow through clearance gaps in cambered hydrofoils. *J. Fluids Eng.* 139 (9), 1–9. doi:10.1115/1.4036269

Conflict of interest

The authors declare that the research was conducted in the absence of any commercial or financial relationships that could be construed as a potential conflict of interest.

Generative AI statement

The author(s) declare that no Generative AI was used in the creation of this manuscript.

Publisher's note

All claims expressed in this article are solely those of the authors and do not necessarily represent those of their affiliated organizations, or those of the publisher, the editors, and the reviewers. Any product that may be evaluated in this article, or claim that may be made by its manufacturer, is not guaranteed or endorsed by the publisher.

Supplementary material

The Supplementary Material for this article can be found online at: <https://www.frontiersin.org/articles/10.3389/fmech.2024.1526120/full#supplementary-material>

- Chitrakar, S., Neopane, H. P., and Dahlhaug, O. G. (2018). "A review on sediment erosion challenges in hydraulic turbines," in *Sedimentation engineering* (InTech). doi:10.5772/intechopen.70468
- Chitrakar, S., Neopane, H. P., and Dahlhaug, O. G. (2019). The numerical and experimental investigation of erosion induced leakage flow through guide vanes of Francis turbine. *IOP Conf. Ser. Earth Environ. Sci.* 240, 072002. doi:10.1088/1755-1315/240/7/072002
- Chitrakar, S., Thapa, B. S., Dahlhaug, O. G., and Neopane, H. P. (2017a). Numerical and experimental study of the leakage flow in guide vanes with different hydrofoils. *J. Comput. Des. Eng.* 4 (3), 218–230. doi:10.1016/j.jcde.2017.02.004
- Chongji, Z., Yexiang, X., Wei, Z., Yangyang, Y., Lei, C., and Zhengwei, W. (2014). Pelton turbine Needle erosion prediction based on 3D three-phase flow simulation. *IOP Conf. Ser. Earth Environ. Sci.* 22, 052019. doi:10.1088/1755-1315/22/5/052019
- Clark, H. M., and Wong, K. K. (1995). Wear Impact angle, particle energy and mass loss in erosion by dilute slurries.
- Dahlhaug, O. G., Skare, P., Mossing, V., and Gutierrez, A. (2010). Erosion resistant coatings for Francis runners and guidevanes. *Int. J. Hydropower and Dams* 2, 109–112.
- De Bree, S. E. M., Rosenbrand, W. F., and de Gee, A. W. J. (1982). "On the erosion resistance in water-sand mixtures of steels for application in slurry pipelines," in *Hydraulic transport of solids in pipes* (Johannesburg: BRHA Fluid Eng).
- Dhanola, A., and Garg, H. C. (2020). *Tribological challenges and advancements in wind turbine bearings: a review*. Elsevier Ltd. doi:10.1016/j.engfailanal.2020.104885
- Divo Bressan, J., Antunes Klemz, M., and Bazanini, G. (2014). *Cavitation erosion damage of metallic materials in rotating disk testing*.
- Ekanger, J. V. (2011). "Morphing skins to improve local flow behavior in a hydro turbine context,". *Master of Science in Energy and Environment submitted on June 2011, Norwegian University of Science and Technology, Department of Energy and Process Engineering*.
- Elkholly, A. (1983). *Prediction of abrasion wear for slurry pump materials*.
- Finnie, I. (1960a). Erosion of surfaces by solid particles. *Wear* 3, 87–103. doi:10.1016/0043-1648(60)90055-7
- Finnie, I. (1960b). *Erosion of surfaces by solid particles*.
- Gajević, S., Marković, A., Milojević, S., Ašonja, A., Ivanović, L., and Stojanović, B. (2024). Multi-objective optimization of tribological characteristics for aluminum composite using Taguchi grey and TOPSIS approaches. *Lubricants* 12 (5), 171. doi:10.3390/lubricants12050171
- Gandhi, B. K., Singh, S. N., and Seshadri, V. (1999). Study of the parametric dependence of erosion wear for the parallel flow of solid-liquid mixtures. Available at: www.elsevier.com/locate/triboint.
- Ge, X., Sun, J., Chu, D., Liu, J., Zhou, Y., Zhang, H., et al. (2023). *Sediment erosion on Pelton turbines: a review*. Springer. doi:10.1186/s10033-023-00880-y
- Ge, X., Sun, J., Zhou, Y., Cai, J., Zhang, H., Zhang, L., et al. (2021). Experimental and numerical studies on opening and velocity influence on sediment erosion of pelton turbine buckets. *Renew. Energy* 173, 1040–1056. doi:10.1016/j.renene.2021.04.072
- Goyal, D. K., Singh, H., Kumar, H., and Sahni, V. (2012). Slurry erosion behavior of HVOF sprayed WC-10Co-4Cr and Al₂O₃+13TiO₂. *Wear* 289, 46–67. doi:10.1016/j.wear.2012.04.016
- Grant, G., and Tabakoff, W. (1973). *An experimental investigation of the erosive characteristics of 2024 aluminum alloy*. Ohio: Cincinnati.
- Grant, I. (1997). Particle image velocimetry: a review. *Proc. Inst. Mech. Eng. C J. Mech. Eng. Sci.* 211 (1), 55–76. doi:10.1243/0954406971521665
- Guo, B., Xiao, Y., Rai, A. K., Liang, Q., and Liu, J. (2021). Analysis of the air-water-sediment flow behavior in Pelton buckets using a Eulerian-Lagrangian approach. *Energy* 218, 119522. doi:10.1016/j.energy.2020.119522
- Guo, B., Xiao, Y., Rai, A. K., Zhang, J., and Liang, Q. (2020). Sediment-laden flow and erosion modeling in a Pelton turbine injector. *Renew. Energy* 162, 30–42. doi:10.1016/j.renene.2020.08.032
- Gupta, R., Singh, S. N., and Sehadi, V. (1995). *Prediction of uneven wear in a slurry pipeline on the basis of measurements in a pot tester*.
- Haugen, K., Ronold, A., and Sandberg, R. (1995). Sand erosion of wear-resistant materials: erosion in choke valves. *Wear* 186–187, 179–188. doi:10.1016/0043-1648(95)07158-x
- Huang, C., Chiovelli, S., Minev, P., Luo, J., and Nandakumar, K. (2008). A comprehensive phenomenological model for erosion of materials in jet flow. *Powder Technol.* 187 (3), 273–279. doi:10.1016/j.powtec.2008.03.003
- Hutchings, I. M. (1981). *A model for the erosion of metals by spherical particles at normal incidence*. Sequoia S. A: Elsevier.
- IEC (2009). *Hydraulic machines e guide for dealing with abrasive erosion in water*. 62364 Ed. 1.0.
- Kang, M. W., Park, N., and Suh, S. H. (2016). "Numerical study on sediment erosion of francis turbine with different operating conditions and sediment inflow rates," in *Procedia engineering* (Elsevier Ltd), 457–464. doi:10.1016/j.proeng.2016.08.389
- Kang, R., and Liu, H. (2020). An integrated model of predicting sand erosion in elbows for multiphase flows. *Powder Technol.* 366, 508–519. doi:10.1016/j.powtec.2020.02.072
- Kapali, A. (2021). *Experimental investigation of sediment erosion in hydraulic turbines*.
- Kapali, A., Chitrakar, S., Shrestha, O., Neopane, H. P., and Thapa, B. S. (2019). A review on experimental study of sediment erosion in hydraulic turbines at laboratory conditions. *J. Phys. Conf. Ser.* 1266, 012016. doi:10.1088/1742-6596/1266/1/012016
- Karthik, S., and Amarendra, H. J. (2019). "Development of slurry jet erosion test rig - an aid to investigate erosion resistance of materials," in *Materials today: proceedings* (Elsevier Ltd), 4426–4430. doi:10.1016/j.matpr.2020.09.674
- Kaunda, C. S., Kimambo, C. Z., and Nielsen, T. K. (2014). *A technical discussion on microhydropower technology and its turbines*. Elsevier Ltd. doi:10.1016/j.rser.2014.04.035
- Kayastha, A., Thapa, B. S., Thapa, B., and Lee, Y. H. (2020). Experimental investigation for R&D in sediment laden pico hydraulic francis turbine. *Renew. Energy* 155, 889–898. doi:10.1016/j.renene.2020.03.116
- Koirala, R., Neopane, H. P., Zhu, B., and Thapa, B. (2019). Effect of sediment erosion on flow around guide vanes of Francis turbine. *Renew. Energy* 136, 1022–1027. doi:10.1016/j.renene.2019.01.045
- Krause, M., and Grein, H. (1996). Abrasion research and prevention. *Hydropower Dams* 4, 17–20.
- Kumar, P., and Saini, R. P. (2010). Study of cavitation in hydro turbines-A review. *Renew. Sustain. Energy Rev.* 14, 374–383. doi:10.1016/j.rser.2009.07.024
- Kumar, R., and Singal, S. K. (2015). "Operation and maintenance problems in hydro turbine material in small hydro power plant," in *Materials today: proceedings* (Elsevier Ltd), 2323–2331. doi:10.1016/j.matpr.2015.07.284
- Kumar Goyal, D., Singh, H., Kumar, H., and Sahni, V. (2012). Slurry erosion behaviour of HVOF sprayed WC-10Co-4Cr and Al₂O₃+13TiO₂ coatings on a turbine steel. *Wear* 289, 46–57. doi:10.1016/j.wear.2012.04.016
- Leguizamón, S., Jahanbakhsh, E., Alimirzazadeh, S., Maertens, A., and Avellan, F. (2019). Multiscale simulation of the hydroabrasive erosion of a pelton bucket: bridging scales to improve the accuracy. *Int. J. Turbomach. Propuls. Power* 4 (2), 9. doi:10.3390/ijtp4020009
- Lin, M. C., Chang, L. S., Lin, H. C., Yang, C. H., and Lin, K. M. (2006). A study of high-speed slurry erosion of NiCrBSi thermal-sprayed coating. *Surf. Coat. Technol.* 201 (6), 3193–3198. doi:10.1016/j.surfcoat.2006.06.040
- Liu, J., Lu, L., and Zhu, L. (2012). Experiment study on sediment erosion of Pelton turbine flow passage component material. *IOP Conf. Ser. Earth Environ. Sci.* 15, 032055. doi:10.1088/1755-1315/15/3/032055
- Liu, J., Yu, J., and Jiang, C. (2019). Evaluation on sediment erosion of Pelton turbine flow passage component. *IOP Conf. Ser. Earth Environ. Sci.* 240, 022027. doi:10.1088/1755-1315/240/2/022027
- Lu, L., Liu, J., Zhang, J. G., Zhu, L., Xu, H. Q., Meng, X. C., et al. (2014). An experiment system for testing synergetic erosion caused by sand abrasion and cavitation. *IOP Conf. Ser. Earth Environ. Sci.* 22, 052017. doi:10.1088/1755-1315/22/5/052017
- Meng, H. C., and Ludema, K. C. (1995). *Wear models and predictive equations: their form and content*. Am Arbor, MI: ELSEVIER Wear.
- Messa, G. V., Mandelli, S., and Malavasi, S. (2019). Hydro-abrasive erosion in Pelton turbine injectors: a numerical study. *Renew. Energy* 130, 474–488. doi:10.1016/j.renene.2018.06.064
- Milojević, S., Savić, S., Mitrović, S., Marić, D., Krstić, B., Stojanović, B., et al. (2023). Solving the problem of friction and wear in auxiliary devices of internal combustion engines on the example of reciprocating air compressor for vehicles. *Teh. Vjesn.* 30 (1), 122–130. doi:10.17559/TV-20220414105757
- Milojević, S., and Stojanović, B. (2018). Determination of tribological properties of aluminum cylinder by application of Taguchi method and ANN-based model. *J. Braz. Soc. Mech. Sci. Eng.* 40 (12), 571. doi:10.1007/s40430-018-1495-8
- Mirza Umar, B., Wang, Z., Chitrakar, S., Thapa, B., Huang, X., Poudel, R., et al. (2024). Experimental erosion flow pattern study of pelton runner buckets using a non-recirculating test rig. *Energies (Basel)* 17 (16), 4006. doi:10.3390/en17164006
- More, S. R., Nandre, B. D., and Desale, G. R. (2014). Development of pot tester to simulate the erosion wear due to solid-liquid mixture. *Int. J. Res. Sci. Dev.* 2 (1). Available at: www.ijrsd.org.
- Morin, G. P., Lavé, J., France-Lanord, C., Rigaudier, T., Gajurel, A. P., and Sinha, R. (2018). Annual sediment transport dynamics in the narayani basin, Central Nepal: assessing the impacts of erosion processes in the annual sediment budget. *J. Geophys. Res. Earth Surf.* 123 (10), 2341–2376. doi:10.1029/2017JF004460
- Naidu, B. S. K. (1997a). Addressing the problems of silt erosion at hydro plants. *Int. J. Hydropower Dams* 4 (3), 72–77.
- Naidu, B. S. K. Addressing the problems of silt erosion at hydro plants (1997b).
- Nakamoto, K., Shiotani, K., Makimoto, M., and Saito, M. (1993). Development of colored stainless steel sheets by ceramics coating. *ISIJ Int.* 33 (9), 968–975. doi:10.2355/isijinternational.33.968

- Neilson, J., and Gilchrist, A. (1968). Erosion by a stream of solid particles. *Wear* 11, 111–122. doi:10.1016/0043-1648(68)90591-7
- Neilson, J. H., and Gilchrist, A. (1967). Erosion by a stream of solid particles. *Wear* 2, 111–122. doi:10.1016/0043-1648(68)90591-7
- Neopane, H. (2010). "Sediment erosion in hydro turbines." PhD Thesis (Trondheim: NTNU).
- Neopane, H. P., Chitrakar, S., and Dahlhaug, O. G. (2019). Role of Turbine Testing Lab for overcoming the challenges related to hydropower development in Nepal. *IOP Conf. Ser. Earth Environ. Sci.* 240, 042012. doi:10.1088/1755-1315/240/4/042012
- Niu, L., Yan, J., and Gao, D. (2020). Research on corrosion and defects of hydraulic metal structures. *IOP Conf. Ser. Earth Environ. Sci.* 455, 012027. doi:10.1088/1755-1315/455/1/012027
- Noon, A. A., and Kim, M. H. (2021). *Sediment and cavitation erosion in Francis turbines—review of latest experimental and numerical techniques*. Basel, Switzerland: MDPI AG. doi:10.3390/en14061516
- Ojala, N., Valtonen, K., Kivikytö-Reponen, P., Vuorinen, P., and Kuokkala, V.-T. (2015). High speed slurry-pot erosion wear testing with large abrasive particles high speed slurry-pot erosion wear testing with large abrasive particles. *TRIBOLOGIA - Finnish J. Tribol.* 1.
- Oka, Y. I., Matsumura, M., and Kawabata, T. (1993). Relationship between surface hardness and erosion damage caused by solid particle impact. *Wear* 162–164, 688–695. doi:10.1016/0043-1648(93)90067-v
- Padhy, M. K., and Saini, R. P. (2009). Effect of size and concentration of silt particles on erosion of Pelton turbine buckets. *Energy* 34, 1477–1483. doi:10.1016/j.energy.2009.06.015
- Padhy, M. K., and Saini, R. P. (2012). Study of silt erosion mechanism in Pelton turbine buckets. *Energy* 39 (1), 286–293. doi:10.1016/j.energy.2012.01.015
- Panic, S., Petrovic, V., Draskovic, S., Kontrec, N., and Milojevic, S. (2023). Performance analysis of hybrid fso/rf communication system with receive diversity in the presence of chi-square/gamma turbulence and rician fading. *Bull. D. Serikbayev EKTU*, 304–312. doi:10.51885/1561-4212_2023_4_304
- Patil, M. S., Patil, M. S., Jahagirdar, R. S., and Jahagirdar, R. S. (2011). "Study of the parameters affecting erosion wear of ductile material in solid-liquid mixture," in *Proceedings of the world congress on engineering* (London: WCE), 1–5.
- Poudel, L., Thapa, B., Shrestha, B. P., Thapa, B. S., Shrestha, K. P., and Shrestha, N. K. (2012). Computational and experimental study of effects of sediment shape on erosion of hydraulic turbines. *IOP Conf. Ser. Earth Environ. Sci.* 15, 032054. doi:10.1088/1755-1315/15/3/032054
- Poudel, R., Shi, J., Zhao, Z., Qian, Z., Guo, Z., Chitrakar, S., et al. (2024). Experimental study of the effects on performance of Francis turbine due to sediments in flow. *J. Phys. Conf. Ser.* 2752, 012207. doi:10.1088/1742-6596/2752/1/012207
- Predescu, C., Berbecaru, A. C., Coman, G., Sohaci, M. G., Predescu, A. M., Matei, E., et al. (2019). Corrosion resistance evaluation of some stainless steels used in manufacture of hydraulic turbine runner blades. *Rev. Chim.* 70, 2491–2496. doi:10.37358/rc.19.7.7367
- Rai, A. K., Kumar, A., and Staubli, T. (2020). Effect of concentration and size of sediments on hydro-abrasive erosion of Pelton turbine. *Renew. Energy* 145, 893–902. doi:10.1016/j.renene.2019.06.012
- Rajkarnikar, B., Neopane, H. P., and Thapa, B. S. (2013). Development of rotating disc apparatus for test of sediment-induced erosion in francis runner blades. *Wear* 306 (1–2), 119–125. doi:10.1016/j.wear.2013.07.011
- Rashed, M. K., Abdulbari, H. A., Salleh, M. A. M., and Ismail, M. H. S. (2016). Rotating disk apparatus: types, developments and future applications. *Mod. Appl. Sci.* 10 (8), 198. doi:10.5539/mas.v10n8p198
- Santa, J. F., Espitia, L. A., Blanco, J. A., Romo, S. A., and Toro, A. (2009). Slurry and cavitation erosion resistance of thermal spray coatings. *Wear* 267 (1–4), 160–167. doi:10.1016/j.wear.2009.01.018
- Sharma, S., and Gandhi, B. K. (2020). Erosion wear behavior of martensitic stainless steel under the hydro-abrasive condition of hydropower plants. *J. Mater. Eng. Perform.* 29 (11), 7544–7554. doi:10.1007/s11665-020-05238-2
- Sharma, S., and Gandhi, B. K. (2021). Experimental investigation of sediment erosion of turbine steel used in Bhilangana-III power-plant. *IOP Conf. Ser. Earth Environ. Sci.* 774, 012108. doi:10.1088/1755-1315/774/1/012108
- Shima, A., Tomaru, H., Ihara, A., and Miura, N. (1992). Cavitation damage study with a rotating disk at the high peripheral velocities. *J. Hydraulic Res.* 30 (4), 521–538. doi:10.1080/00221689209498898
- Shimizu, K., Naruse, T., Xinba, Y., Kimura, K., Minami, K., and Matsumoto, H. (2009). Erosive wear properties of high V-Cr-Ni stainless spheroidal carbides cast iron at high temperature. *Wear* 267 (1–4), 104–109. doi:10.1016/j.wear.2008.12.086
- Shrestha, O., Kapali, A., Thapa, B., Neopane, H. P., and Lee, Y.-H., "Rotating disc apparatus (RDA) for estimation of erosion in micro crossflow hydro turbines." 2021.
- Stachowiak, G. W., and Batchelor, A. W. (2006). *Engineering tribology*. 3rd ed. Butterworth – Heinemann, Elsevier.
- Tarodiya, R., and Gandhi, B. K. (2019). Experimental investigation on slurry erosion behavior of 304L steel, grey cast iron, and high chromium white cast iron. *J. Tribol.* 141 (9). doi:10.1115/1.4043903
- Thapa, B. S. (2016). "Effects of sediment erosion in guide vanes of Francis turbines." Doctoral thesis (Trondheim: Norwegian University of Science and Technology).
- Thakur, R., Khurana, S., Thakur, R., Kumar, A., Nadda, R., and Sethi, M. (2017a). Experimental study and optimizing erosive wear rate parameters using A novel entropy vikor approach in A pelton turbine buckets. *Int. J. Mech. Eng. Technol. (IJMET)* 8 (6), 27–43. Available at: <http://www.iaeme.com/IJMET/index.asp27>.
- Thakur, R., Kumar, A., Khurana, S., and Sethi, M. (2017b). Correlation development for erosive wear rate on pelton turbine buckets. *Int. J. Mech. Prod. Eng. Res. Dev.* 7 (3), 259–274. doi:10.24247/ijmperdjun201727
- Thapa, B. (2004a). "Sand erosion in hydraulic machinery." PhD Thesis (Trondheim: NTNU).
- Thapa, B., "Sand erosion in hydraulic machinery," 2004b.
- Thapa, B., Chaudhary, P., Dahlhaug, O. G., and Upadhyay, P. (2007). "Study of combined effect of sand erosion and cavitation in hydraulic turbines," in *International conference on small hydropower-hydro Sri Lanka* (Sri Lanka).
- Thapa, B., Shrestha, R., Dhakal, P., and Thapa, B. S. (2005). Sediment in Nepalese hydropower projects. *J. Aquat. Ecosyst. Health Manage* 8 (3), 251258.
- Thapa, B., Thapa, B. S., Dahlhaug, O. G., and Shrestha, K. P. (2012b). "Accelerated testing for resistance to sand erosion in hydraulic turbines," in *International conference on water resources and renewable energy development in asia, Thailand*.
- Thapa, B. S., Dahlhaug, O. G., and Thapa, B. (2017). Effects of sediment erosion in guide vanes of Francis turbine. *Wear* 390–391, 104–112. doi:10.1016/j.wear.2017.07.012
- Thapa, B. S., Dahlhaug, O. G., and Thapa, B. (2018). Flow measurements around guide vanes of Francis turbine: a PIV approach. *Renew. Energy* 126, 177–188. doi:10.1016/j.renene.2018.03.042
- Thapa, B. S., Thapa, B., and Dahlhaug, O. G. (2012a). Empirical modelling of sediment erosion in Francis turbines. *Energy* 41 (1), 386–391. doi:10.1016/j.energy.2012.02.066
- Thapa, B. S., Trivedi, C., and Dahlhaug, O. G. (2016). Design and development of guide vane cascade for a low speed number Francis turbine. *J. Hydrodynamics* 28 (4), 676–689. doi:10.1016/S1001-6058(16)60648-0
- Tsai, W., Humphrey, J. A. C., Cornet, L., and V Levy, A. (1981). *Experimental measurement of accelerated erosion in a slurry pot tester*. Elsevier Sequoia S.A.
- Tsuguo, N. (1999). "Estimation of repair cycle of turbine due to abrasion caused by suspended sand and determination of desilting basin capacity," in *Proceedings of international seminar on sediment handling technique* (Kathmandu: NHA).
- Turenne, S., Fiset, M., and Masounave, J. (1989). The effect of sand concentration on the erosion of materials by a slurry jet. *J. Wear* 133, 95–106. doi:10.1016/0043-1648(89)90116-6
- Veerabhadra Rao, P., Syamala Rao, B., and Lakshmana Rao, N. (1980). Erosion and cavity characteristics in rotating components. *J. Test. Eval.* 8 (3), 127–142. doi:10.1520/jte10609j
- Vivekananda, P. (1983). "Mechanism of cavitation damage influence of stacking fault energy on erosion and erosion resistance of steels and coatings." PhD Thesis (Bangalore, India: Indian Institute of Science).
- Winkler, K. (2014). Hydro-abrasive erosion: problems and solutions. *IOP Conf. Ser. Earth Environ. Sci.* 22, 052022. doi:10.1088/1755-1315/22/5/052022
- Wiederhorn, S. M., and Hockey, B. J., "Effect of material parameters on the erosion resistance of brittle materials," 1983.
- William, J. S. (1987). *Ball mill and hub test methods for slurry erosion evaluation of materials*. Middletown, Ohio: Armco, Inc., 5–16. doi:10.1520/STP19411S
- Wood, R. J. K. (1999). The sand erosion performance of coatings. *Mater. Des.* 20, 179–191. doi:10.1016/s0261-3069(99)00024-2
- Wood, R. J. K., and Wheeler, D. W. (1998). Design and performance of a high velocity air-sand jet impingement erosion facility. *Wear* 220, 95–112. doi:10.1016/s0043-1648(98)00196-3
- Wu, J., Graham, L., Lester, D., Wong, C., Kilpatrick, T., Smith, S., et al. (2011). An effective modeling tool for studying erosion. *Wear* 270 (9–10), 598–605. doi:10.1016/j.wear.2011.01.016
- Yan, C., Chen, W., Zhao, Z., and Liu, L. (2020). A probability prediction model of erosion rate for Ti-6Al-4V on high-speed sand erosion. *Powder Technol.* 364, 373–381. doi:10.1016/j.powtec.2020.01.058
- Zhang, H. M., and Zhang, L. X. (2014). Numerical investigation of sediment-laden flow in a high-head francis turbine runner. *Adv. Mater. Res.* 860–863, 1542–1546. doi:10.4028/www.scientific.net/AMR.860-863.1542
- Zhang, J., Richardson, M. O. W., Wilcox, G. D., Min, J., and Wang, X. (1996). *WEAR Assessment of resistance of non-metallic coatings to silt abrasion and cavitation erosion in a rotating disk test rig*.
- Zhiye, J. (1983). *An experimental investigation on cavitation erosion for propeller alloys*. China.
- Zu, J. B., Ihtchings, I. M., and Burstein, G. T. (1990). Design of a slurry erosion test rig. *Wear* 140, 331–344. doi:10.1016/0043-1648(90)90093-p